

The Lattice Boltzmann Equation Method: Theoretical Interpretation, Numerics and Implications

R.R. Nourgaliev, T.N. Dinh, T.G. Theofanous, and D. Joseph[‡]

Center for Risk Studies and Safety, University of California, Santa Barbara, USA

[‡]*Aerospace Engineering and Mechanics, University of Minnesota, USA*

E-mail: robert@crss.ucsb.edu; nam@crss.ucsb.edu; theo@theo.ucsb.edu; joseph@aem.umn.edu

During the last ten years the Lattice Boltzmann Equation (LBE) method has been developed as an alternative numerical approach in computational fluid dynamics (CFD). Originated from the discrete kinetic theory, the LBE method has emerged with the promise to become a superior modeling platform, both computationally and conceptually, compared to the existing arsenal of the continuum-based CFD methods. The LBE method has been applied for simulation of various kinds of fluid flows under different conditions. The number of papers on the LBE method and its applications continues to grow rapidly, especially in the direction of complex and multiphase media.

The purpose of the present paper is to provide a comprehensive, self-contained and consistent tutorial on the LBE method, aiming to clarify misunderstandings and eliminate some confusion that seems to persist in the LBE-related CFD literature. The focus is placed on the fundamental principles of the LBE approach. An excursion into the history, physical background and details of the theory and numerical implementation is made. Special attention is paid to advantages and limitations of the method, and its perspectives to be a useful framework for description of complex flows and interfacial (and multiphase) phenomena. The computational performance of the LBE method is examined, comparing it to other CFD methods, which directly solve for the transport equations of the macroscopic variables.

CONTENTS

1. *Introduction .*
2. *Origin and basic idea of the lattice Boltzmann equation method .*
3. *Numerical implementation of the LBE method .*
4. *Lattice Boltzmann models for hydrodynamics of complex fluids .*
5. *Derivation and analysis of the continuum equivalent of the LB equation .*
6. *Computational efficiency .*
7. *Concluding remarks .*
 - A. *Lattice geometry and symmetry.*
 - B. *Equilibrium distribution function.*
 - C. *Multiphase flow modeling.*
 - D. *Derivation of the viscous stress tensor for the LBGK models.*
 - E. *Evaluation of the deviations from the Navier-Stokes equations.*

1. INTRODUCTION

From its birth over 10 years ago [69], the lattice Boltzmann Equation (LBE) method has been aggressively pursued and at a pace that is strongly accelerating in the past few years. The method has found application in different areas of computational fluid dynamics (CFD), including simulation of flows in porous media; non-ideal, binary and ternary complex fluids; microfluidics; particulate and suspension flows; to name but a few (see for review [84] and [16]). Proponents of the LBE method consider the method to possess potentials to become a versatile CFD platform that is superior over the existing, continuum-based CFD methods. At the same time, since the method, and its variants and extensions, are still being formulated and improved, the diverse and growing body of the LBE literature suffers from controversy and lack of distillation. In our opinion, the situation has become unhealthy and actually caused unnecessary confusion. In addition, overstatement of the method capabilities formed a ground for criticism. We feel a strong need for clarification and a consistent presentation of the LBE methodology, its technology, terminology and features on a basis that eventually eliminates further misunderstandings and misuse of the method. More importantly, we feel that a fair and careful assessment of the LBE method features would help those who enter the field to develop a realistic view about the method's capabilities and limitations.

With this in mind, we organize this paper as a comprehensive tutorial. It starts from the discussion of the fundamental principles and origin of the approach, section 2, which includes short introduction of the kinetic theory of gases and its connection to the LBE method. Next, practical implementation of the LBE algorithms is discussed in section 3. Hydrodynamic models of the LBE method are then introduced in much greater details in section 4, where an assessment of the models is also provided. Special attention is paid to the capability and limitations of the LBE models to simulate fluid-fluid multiphase flows and fluid-fluid interfaces. Section 5 presents a Chapman-Enskog analysis of the discrete Boltzmann equation; and derivation and discussion of the hydrodynamic equations for three most commonly used LBE models. Section 6 provides a comparative analysis of the method in terms of simplicity and efficiency of algorithms, and potentials for effective parallelization. The paper concludes with a summary about the method applicability and perspectives.

2. ORIGIN AND BASIC IDEA OF THE LATTICE BOLTZMANN EQUATION METHOD

2.1. Boltzmann equation and kinetic theory of gases

The purpose of this section is to outline the most important facts and results of the kinetic theory which are relevant to the lattice Boltzmann equation method. More exhaustive overview of the kinetic theory and recent important developments can be found in [15]; [49]; [55]; [64]; [14]; [39]; [57] and [21].

Kinetic theory. The Lattice Boltzmann Equation method originates from the kinetic theory of gases. The primary variable of interest is a one-particle probability distribution function (PPDF), $f(\mathbf{r}, \mathbf{e}, t)$, so defined that $[f(\mathbf{r}, \mathbf{e}, t) \cdot d^3 r \cdot d^3 e]$ is the number of particles which, at time t , are located within a phase-space control element $[d^3 r \cdot d^3 e]$ about \mathbf{r} and \mathbf{e} (\mathbf{r} is a particle's coordinate in physical space and \mathbf{e} is a particle's velocity). The transport equation for the PPDF can be expressed as [49]:

$$(\partial_t + \mathbf{e} \cdot \nabla_{\mathbf{r}} + \mathbf{a} \cdot \nabla_{\mathbf{e}}) f(\mathbf{r}, \mathbf{e}, t) = (\partial_t f)_{\text{coll}} \quad (1)$$

where \mathbf{a} is the external force acting on the particle.

Boltzmann equation. To derive the Boltzmann equation from equation (1), the collision term $(\partial_t f)_{\text{coll}}$ has to be explicitly specified. Two major assumptions were made [49]: (a) only binary collisions are taken into account. This is valid if the gas is sufficiently dilute (ideal gas). (b) The velocity of a molecule is uncorrelated with its position¹. The last assumption is known as the *assumption of molecular chaos*. Importantly, without this assumption, the collision operator $(\partial_t f)_{\text{coll}}$ would not be expressible in terms of f itself. Instead, it would involve a two-particle probability distribution function. In general case, equation (1) can be replaced by a set of N coupled equations to account for multi-particle interactions (BBGKY equations).

Under the assumptions made, Boltzmann [12] expressed the collision term of equation (1) as² [15] [49] [55]:

$$(\partial_t f)_{\text{coll}} = \int d\Omega \int d^3 e^{(0)} \sigma(\Omega) \left| \mathbf{e} - \mathbf{e}^{(0)} \right| \left(f' f'^{(0)} - f f^{(0)} \right) \quad (2)$$

where Ω is the scattering angle of the binary collision $\{\mathbf{e}', \mathbf{e}'^{(0)}\} \rightarrow \{\mathbf{e}, \mathbf{e}^{(0)}\}$ with fixed \mathbf{e} ; f and f' denote the PPDF before and after collision; and $\sigma(\Omega)$ is the differential cross section of this collision, [49].

¹ In fact, two other assumptions were also made: (c) wall effects are ignored and (d) the effect of the external force on the collision cross section is neglected.

² Boltzmann's derivation of the collision integral, eq.(2), was, even though intuitive, deeply insightful. There is a gap between Newton's equations of motion of the molecules constituting a gas and the Boltzmann equation (2). Nevertheless, this equation is known to be valid, and it has been successfully applied to study transport properties of dilute gases [55]. A more general BBGKY theory (due to Bogoliubov, 1946 [11], Kirkwood, 1947 [54], and Grad, 1949 [35]) was developed to provide a consistent derivation of the Boltzmann equation.

Boltzmann's ‘ \mathbb{H} theorem’. Introducing the functional \mathbb{H} as the complete integral defined by the equation

$$\mathbb{H} = \int f \ln f \, d\mathbf{e} \quad (3)$$

the Boltzmann ‘ \mathbb{H} theorem’ states that if the PPDF, f , satisfies the Boltzmann transport equation (1) and (2), then \mathbb{H} is a non-increasing in time function, $\frac{d\mathbb{H}(t)}{dt} \leq 0$. This is the analog of the second law of thermodynamics, if we identify \mathbb{H} with the negative of the entropy per unit volume divided by Boltzmann's constant, $\mathbb{H} = -\frac{S}{Vk_B}$. Thus, the ‘ \mathbb{H} theorem’ states that, for a fixed volume V , the entropy never decreases, [12] and [49].

Collision interval theory. The collision integral, eq.(2), can be significantly simplified for near-equilibrium states. The collision interval theory states that during time interval δ_t a fraction $\delta_t/\tau = \frac{1}{\tau^*}$ of the particles in a given small volume undergoes collisions, which alter the PPDF from f to the equilibrium value given by the Maxwellian:

$$f^{\text{eq}} = \frac{\rho}{(2\pi RT)^{\mathcal{D}_0/2}} \exp \left[-\frac{(\mathbf{e} - \mathbf{u})^2}{2RT} \right] \quad (4)$$

where \mathcal{D}_0 , R , T , ρ and \mathbf{u} are the dimension of space, gas constant, temperature, macroscopic density and velocity, respectively. Thus, the collision term can be expressed in the form known as the ‘BGK collision operator’, [7] and [15]:

$$(\partial_t f)_{\text{coll}} = -\frac{f - f^{\text{eq}}}{\tau} = -\frac{f - f^{\text{eq}}}{\delta_t \tau^*} \quad (5)$$

where τ is a relaxation time^{3,4}. The Boltzmann equation with the BGK collision operator has the following form:

$$\partial_t f + \mathbf{e} \cdot \nabla_{\mathbf{r}} f + \mathbf{a} \cdot \nabla_{\mathbf{e}} f = -\frac{f - f^{\text{eq}}}{\tau} \quad (6)$$

Simplification of the forcing term. In order to evaluate the forcing term, the derivative $\nabla_{\mathbf{e}} f$ has to be explicitly given. The following assumption is made [44]:

$$\nabla_{\mathbf{e}} f \approx \nabla_{\mathbf{e}} f^{\text{eq}} \quad (7)$$

which is due to the fact that f^{eq} is the leading part of the distribution function f (‘an assumption of small deviation from the equilibrium’). By combining the Maxwellian eq.(4) with eq.(7) and eq.(6), the following equation is obtained:

$$\partial_t f + \mathbf{e} \cdot \nabla_{\mathbf{r}} f = -\frac{f - f^{\text{eq}}}{\tau} + \frac{\mathbf{a} \cdot (\mathbf{e} - \mathbf{u})}{RT} f^{\text{eq}} \quad (8)$$

³The BGK equation (5) is a *phenomenological equation* [64]. This characteristic pre-determines the domain of the equation's applicability: dilute gases in a state close to thermal equilibrium. The inaccuracy of the BGK equation is enhanced when one treats the equation by the Chapman-Enskog method [55].

⁴The ‘ \mathbb{H} theorem’ remains valid for the BGK equation, [55].

Link to hydrodynamics. Connection of the Boltzmann equation to the hydrodynamics is accomplished through the integration in the particle momentum space:

$$\begin{aligned} \rho &= \int [f] d\mathbf{e}; & \rho \mathbf{u} &= \int [f \cdot \mathbf{e}] d\mathbf{e}; & \rho \mathcal{E} &= \frac{1}{2} \int [f \cdot (\mathbf{e} - \mathbf{u})^2] d\mathbf{e} \\ \rho &= \int [f^{\text{eq}}] d\mathbf{e}; & \rho \mathbf{u} &= \int [f^{\text{eq}} \cdot \mathbf{e}] d\mathbf{e}; & \rho \mathcal{E} &= \frac{1}{2} \int [f^{\text{eq}} \cdot (\mathbf{e} - \mathbf{u})^2] d\mathbf{e} \end{aligned} \quad (9)$$

with the kinetic energy \mathcal{E} given by

$$\mathcal{E} = \frac{\mathcal{D}_0}{2} k_B T = \frac{\mathcal{D}_0}{2} \frac{RT}{N_A} \quad (10)$$

where N_A and k_B are the Avogadro's (or Loschmidt's [15]) number and the Boltzmann constant, respectively. \mathcal{D}_0 is the number of degrees of freedom of a particle ($\mathcal{D}_0 = 3$ and 5 for monoatomic and diatomic gases, respectively).

2.2. Lattice Boltzmann equation

2.2.1. Heuristic approach

Historically, the ‘classical’ LB equation has been developed empirically, with basic idea borrowed from the cellular automata fluids, [31] and [103]. The physical space of interest is filled with regular lattice populated by discrete particles. Particles ‘jump’ from one site of the lattice to another with discrete particle velocities \mathbf{e}_a , ($a = 0, \dots, b$, where b is the total number of possible molecule's directions), and colliding with each other at the lattice nodes, Figs.1a,1b. The lattice geometry (a set of possible particle velocities) should obey certain symmetry requirements (see Appendix A), which are compelling in order to recover the rotational invariance of the momentum flux tensor at the macroscopic level [103].

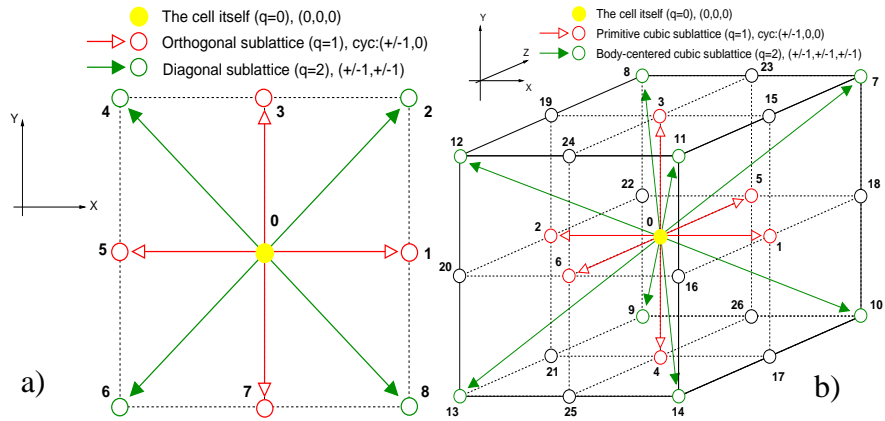


FIG. 1a. Lattice geometry and velocity vectors of the two-dimensional nine-speed D_2Q_9 model.

FIG. 1b. Lattice geometry and velocity vectors of the three-dimensional fifteen-speed D_3Q_{15} model.

In effect, the LBE method corresponds to the following formal discretization in the phase space of the Boltzmann equation:

$$\begin{aligned} \text{a) } f &\rightarrow f_a \\ \text{b) } \mathbf{e} &\rightarrow \mathbf{e}_a \\ \text{c) } f^{\text{eq}} &\rightarrow f_a^{\text{eq}} = A_a + B_a e_{a_i} u_i + C_a u^2 + D_a e_{a_i} e_{a_j} u_i u_j \end{aligned} \quad (11)$$

where the discrete equilibrium distribution function, also called “the Chapman-Enskog expansion”, is inspired by the following constant-temperature and small velocity (low-Mach-number) approximation of the Maxwellian eq.(4)

$$f^{\text{eq}} \approx \frac{\rho \cdot \exp\left[-\frac{\mathbf{e}^2}{2RT}\right]}{(2\pi RT)^{D_0/2}} \times \left\{ 1 + \frac{(\mathbf{e} \cdot \mathbf{u})}{RT} + \frac{(\mathbf{e} \cdot \mathbf{u})^2}{2(RT)^2} - \frac{u^2}{2RT} \right\} + \mathcal{O}(u^3) \quad (12)$$

Thus, the lattice Boltzmann BGK equation is heuristically postulated as⁵

$$\underbrace{\partial_t f_a + e_{a_j} \partial_j f_a}_{\text{Advection operator, } \mathcal{A}(f_a)} = - \underbrace{\frac{f_a - f_a^{\text{eq}}}{\tau} + \frac{a_j \cdot (e_{a_j} - u_j)}{RT} f_a^{\text{eq}}}_{\text{Collision operator, } \Omega(f_a)} \quad (13)$$

As a next step, one can define the “LBE sound speed” as [43]

$$c_s \equiv \sqrt{RT} \quad (14)$$

At this point, a principal departure from the actual kinetic theory must be emphasized.

- According to the kinetic theory [15], the speed of sound is related to the temperature as

$$c_s = \sqrt{\gamma RT} \quad (15)$$

where $\gamma = \frac{c_p}{c_v} = 1 + \frac{2}{D_0}$ is a ratio of specific heats. The definition eq.(14) means that the LBE’s pseudo-molecules must have infinite number of degrees of freedom, $D_0 = \infty$, which, of course, does not make any physical sense.

Remark 1:

- As we show further below (section 3.3), if the fluid being modeled is to retain its speed of sound, the solution of eq.(13) is impossible for all practical purposes. As a consequence, compressibility effects are outside the realm of the LBE method; c_s is retained, however, with a totally different meaning and role - that of a pseudo-compressibility parameter that allows the solution to relax to the appropriate incompressible viscous solution.

Rather than “sound speed”, let us call, therefore, c_s by the name “*Pseudo-Sound-Speed*” (“PSS”). Furthermore, as a consequence, the relaxation time and related molecular mean free path and velocity also change their meaning and they would be called as “*Lattice relaxation time*”, “*Lattice mean free path*” and “*Lattice velocity*”, respectively. While this departs from the normal usage, adoption of these terms, we believe, will clear up an enormous conceptual barrier for the newcomers and uninitiated.

⁵We have limited our study to the BGK LBE models, which are currently in the mainstream of the LBE technology. There are several non-BGK LBE models available in the literature. McNamara et al. pursue an approach with multi-particle collision operator [70]; [71] and [72]. Similar approach is utilized by Eggels and Somers ([25] and [26]). Another recent development of the non-BGK LBE is due to Lallemand and Luo, [60]. While being more sophisticated both conceptually and technically, these models are believed to be more stable and more flexible in implementation of variable fluid properties.

The coefficients A_a , B_a , C_a and D_a of the ‘Chapman-Enskog’ expansion for f_a^{eq} , eq.(11), are ‘tuned’ to recover mass, momentum conservation and viscous stress tensor during the multiscale Chapman-Enskog perturbative expansion procedure⁶.

Eqs.(13) are the coupled system of Hamilton-Jacobi equations, with Hamiltonian $e_{a_j} \partial_j f_a$, and the ‘coupling’ source term given by the collision operator. This system can be solved by any appropriate numerical scheme (see section 3).

2.2.2. Consistent discretization

Recent studies by He and Luo [42] [43] pioneer another way to establish the LBE methodology. In particular, He and Luo [43] demonstrated that the lattice Boltzmann equation can be viewed as a *special finite-difference approximation* of the Boltzmann equation. The chief idea and motivation are to provide a sound theoretical foundation for a transition from the ‘continuous’ Boltzmann equation to the LBE, which involves the choice of the discrete particle velocities (structure of the lattice) and the choice of the coefficients of expansion for equilibrium distribution function, eq.(11). There are two major ingredients in the procedure by He and Luo, discussed below.

Time discretization. Eq.(6) is integrated over a time step δ_t :

$$f(\mathbf{r} + \mathbf{e} \cdot \delta_t, \mathbf{e}, t + \delta_t) - f(\mathbf{r}, \mathbf{e}, t) = - \int_t^{t+\delta_t} \frac{f - f^{\text{eq}}}{\tau} dt + \int_t^{t+\delta_t} \frac{\mathbf{a} \cdot (\mathbf{e} - \mathbf{u})}{RT} f^{\text{eq}} dt \quad (16)$$

The first integral in the collision operator is treated explicitly, using the first-order approximation, while the second one can be treated using the trapezoidal implicit scheme [44], which, in order to regain the explicitness of the method, entails the following variable transformation:

$$h = f - \frac{\mathbf{a} \cdot (\mathbf{e} - \mathbf{u})}{2RT} f^{\text{eq}} \delta_t \quad (17)$$

Thus, the first-order time discretization yields the following Boltzmann equation:

$$h(\mathbf{r} + \mathbf{e} \cdot \delta_t, \mathbf{e}, t + \delta_t) - h(\mathbf{r}, \mathbf{e}, t) = - \frac{h(\mathbf{r}, \mathbf{e}, t) - h^{\text{eq}}(\mathbf{r}, \mathbf{e}, t)}{\tau} \delta_t \quad (18)$$

where $h^{\text{eq}} = \left[1 - \frac{\mathbf{a} \cdot (\mathbf{e} - \mathbf{u})}{2c_s^2} \delta_t \right] f^{\text{eq}}$

Note, that the speed of sound is defined by eq.(14).

Phase space discretization. This step establishes the structure of the lattice and the form of the equilibrium distribution function. To derive a ‘consistent’ LBE scheme, the integration in momentum space eq.(9) has to be approximated by the following quadrature [43]:

$$\int \psi(\mathbf{e}) f^{\text{eq}}(\mathbf{r}, \mathbf{e}, t) d\mathbf{e} \approx \sum_a \mathcal{W}_a \psi(\mathbf{e}_a) f_a^{\text{eq}}(\mathbf{r}, \mathbf{e}_a, t) \quad (19)$$

⁶In the case of the ‘thermal’ LBE, it is also required to conserve energy, which would entail addition of the expansion terms in the Taylor series eqs.(11) and (12).

where $\psi(\mathbf{e}) = [1; e_i; (e_i e_j); (e_i e_j e_k); \dots]$ and \mathcal{W}_a are the polynomials of \mathbf{e} and the ‘weight’ coefficient of the quadrature, respectively. Eq.(19) corresponds to the following ‘link’ of the LBE to hydrodynamics⁷:

$$\begin{aligned} \rho &= \sum_a f_a; & \rho \mathbf{u} &= \sum_a f_a \cdot \mathbf{e}_a; & \rho \mathcal{E} &= \frac{1}{2} \sum_a f_a \cdot (\mathbf{e}_a - \mathbf{u})^2 \\ \rho &= \sum_a f_a^{\text{eq}}; & \rho \mathbf{u} &= \sum_a f_a^{\text{eq}} \cdot \mathbf{e}_a; & \rho \mathcal{E} &= \frac{1}{2} \sum_a f_a^{\text{eq}} \cdot (\mathbf{e}_a - \mathbf{u})^2 \end{aligned} \quad (21)$$

where

$$f_a(\mathbf{r}, t) \equiv \mathcal{W}_a f(\mathbf{r}, \mathbf{e}_a, t); \quad f_a^{\text{eq}}(\mathbf{r}, t) \equiv \mathcal{W}_a f^{\text{eq}}(\mathbf{r}, \mathbf{e}_a, t) \quad (22)$$

Now, a task is to properly specify the abscissas of the quadrature eq.(19), or, in other words, the ‘structure’ (‘symmetry’) of the lattice. To do that, one must impose a set of constraints for this ‘structure’. These constraints are formulated based on the Chapman-Enskog procedure to ‘link’ the Boltzmann equation to the Navier-Stokes equations, see section 5.1, which involves the following moments of the equilibrium distribution function:

$$\begin{aligned} \text{Mass conservation:} & \quad \psi(\mathbf{e}) = 1; \quad e_i; \quad \text{and} \quad e_i e_j \\ \text{Momentum conservation:} & \quad \psi(\mathbf{e}) = 1; \quad e_i; \quad e_i e_j; \quad \text{and} \quad e_i e_j e_k \\ \text{Energy conservation:} & \quad \psi(\mathbf{e}) = 1; \quad e_i; \quad e_i e_j; \quad e_i e_j e_k; \quad \text{and} \quad e_i e_j e_k e_l \end{aligned} \quad (23)$$

Thus, the basic idea is that with the chosen abscissas of the quadrature eq.(19), the moments of f_a^{eq} , eq.(23), should be calculated exactly. With this, the Chapman-Enskog procedure is intact, and it is argued that the framework of the lattice Boltzmann equation can rest on that of the Boltzmann equation, and the rigorous results of the Boltzmann equation can be extended to the LBE via this explicit connection [42].

Remark 2:

It is instructive to note that the Maxwell-Boltzmann equilibrium distribution function f^{eq} is an exact solution of the Chapman-Enskog zero-order approximation of the Boltzmann equation [49]. In finding the abscissas of the quadrature eq.(19), however, instead of the exact Maxwellian, its constant-temperature and low-Mach-number approximation eq.(12) is utilized, [43], with which no rigorous link to the Navier-Stokes equations is available. Moreover, this is exactly the reason why the Boltzmann’s “H” theorem does not hold for the LBE. Therefore, this procedure does not provide a substitute for the Chapman-Enskog multiscale perturbative expansion procedure (see section 5.1)

The details of the procedure to find the required abscissas of the quadrature and corresponding approximations of the Maxwellian are given in [43] for two-dimensional 6-, 7- and 9-bit and three-dimensional 27-bit lattice models. It is important to note that with this procedure, the ‘weighting’ coefficients for the ‘composing’ sublattices and the coefficients of the equilibrium distribution function are exactly the same as those of the ‘heuristic’ LBE,

⁷ In the case of the transformation eq.(17), f is substituted by h , and the first momentum is modified as

$$\rho \mathbf{u} - \frac{1}{2} \rho \mathbf{a} \delta t = \int [h \cdot \mathbf{e}] d\mathbf{e}; \quad \rho \mathbf{u} - \frac{1}{2} \rho \mathbf{a} \delta t = \int [h^{\text{eq}} \cdot \mathbf{e}] d\mathbf{e} \quad (20)$$

summarized in Appendices A and B, providing that⁸ $c_s^2 = \frac{\Upsilon^{(4)}}{\Upsilon^{(2)}}$, [45].

2.2.3. Non-dimensional form

To cast the discrete Boltzmann equation (13) into the non-dimensional form, one must introduce the following characteristic scales⁹:

Characteristic length scale:	L	
Characteristic velocity:	U_0	
Reference density:	ρ_r	(24)
Lattice mean free path:	λ	

Using these scales, the variables utilized in the LBE theory are non-dimensionalized as

<i>Non-dimensional variables:</i>		
<i>PPDF:</i>	\hat{f}_a	$= \frac{f_a}{\rho_r}$
<i>Lattice velocity:</i>	$\hat{e}_{a,i}$	$= \frac{e_{a,i}}{U_0}$
<i>Time:</i>	\hat{t}	$= \frac{t U_0}{L}$
<i>Length:</i>	$\hat{\mathbf{r}}$	$= \frac{\mathbf{r}}{L}$
<i>Density:</i>	$\hat{\rho}$	$= \frac{\rho}{\rho_r}$
<i>Macroscopic velocity:</i>	\hat{u}_i	$= \frac{u_i}{U_0}$
<i>Pseudo-sound-speed:</i>	\hat{c}_s	$= \frac{c_s}{U_0}$
<i>Body force:</i>	\hat{a}_j	$= \frac{a_j L}{U_0^2} = \frac{i_j}{Fr}$
<i>Kinematic viscosity:</i>	$\hat{\nu}$	$= \frac{\nu}{U_0 L} = \frac{1}{Re}$

where \mathbf{i} is a unit-vector, specifying the direction of the body forces.

To make a non-dimensional relaxation time, we will use the lattice Knudsen number defined as a ratio of the lattice mean free path λ to the flow characteristic length scale L :

$$\varepsilon = \frac{\lambda}{L} \quad (26)$$

Defining the “collision time” as $t_c \equiv \frac{\lambda}{U_0}$, the dimensionless relaxation time is

$$\hat{\tau} = \frac{\tau}{t_c} = \frac{\tau U_0}{\lambda} = \frac{U_0}{e_m} \quad (27)$$

where the scaling “lattice-molecular velocity” is defined as $e_m \equiv \frac{\lambda}{\tau}$.

⁸In the ‘heuristic’ LBE models, the lattice symmetry parameters $\Upsilon^{(4)}$ and $\Upsilon^{(2)}$ are adjustable, with free parameter w_0 , allowing to vary the pseudo-sound-speed. For D_2Q_9 , the requirement $c_s^2 = \frac{\Upsilon^{(4)}}{\Upsilon^{(2)}}$ is satisfied with $w_0 = \frac{4}{9}$.

⁹As explained in Remark 1, we add the ‘prefix’ “lattice”, emphasizing the artificial nature of the LBE’s “pseudo-molecules”; and, correspondingly, of the LBE’s mean free path, sound speed, etc.

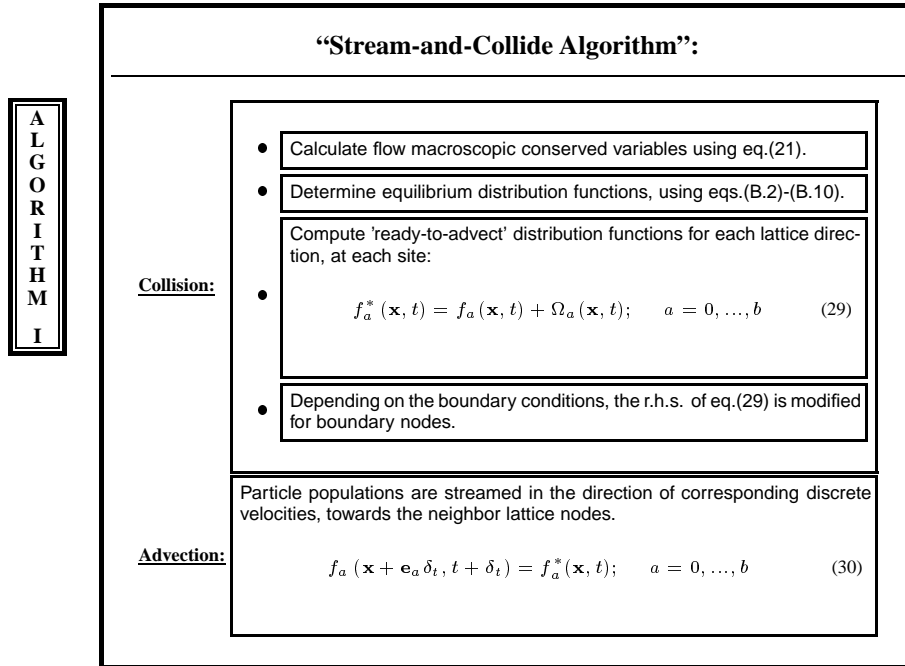
With this dimensionalization introduced, the discrete Boltzmann equation (13) is transformed into the following non-dimensional equation:

$$\partial_t \hat{f}_a + \hat{e}_{a_j} \partial_j \hat{f}_a = -\frac{\hat{f}_a - \hat{f}_a^{\text{eq}}}{\varepsilon \hat{\tau}} + \frac{\hat{a}_j \cdot (\hat{e}_{a_j} - \hat{u}_j)}{\hat{c}_s^2} \hat{f}_a^{\text{eq}} \quad (28)$$

For the most of the paper, for compactness, the hat $\hat{(\cdot)}$ is omitted; and, unless explicitly specified, all variables are assumed to be non-dimensional.

3. NUMERICAL IMPLEMENTATION OF THE LBE METHOD

In the present section, we will describe the basic numerical algorithms for solution of the LBE equation (28). We will start with the “stream-and-collide” algorithm (section 3.1), which is utilized in most LBE simulations. Then, in section 3.2, several other algorithms are described, which have been found useful to overcome stability problems, attributed to the “stream-and-collide scheme”.



3.1. Basic “stream-and-collide” algorithm

Eq.(28) is a system of $(b + 1)$ one-dimensional¹⁰ PDE Hamilton-Jacobi equations for scalars $\vartheta = f_a$, ($a = 0, \dots, b$), consisting of an “advection part”, $\mathcal{A}(\vartheta)$, and a “collision

¹⁰Note, for each a^{th} -equation, the axis $X = x_a$ of the coordinate system is “pointing” in the direction of the vector \mathbf{e}_a .

part”, $\Omega(\vartheta)$:

$$\underbrace{\frac{\partial \vartheta}{\partial t} + \frac{\delta}{\delta_t} \frac{\partial \vartheta}{\partial X}}_{\mathcal{A}(\vartheta)} = \frac{\Omega(\vartheta)}{\delta_t} \quad (31)$$

where $\delta (= \delta_a)$ is a step of space discretization in $X (= x_a)$ -direction; and the collision operator is $\Omega(\vartheta) \equiv -\frac{f_a - f_a^{\text{eq}}}{\tau^*}$.

The simplest scheme for discretization of each of these equations involves a first-order-accurate implicit forward differencing for the advection part,

$$\mathcal{A}(\vartheta) = \frac{\vartheta_i^{(n+1)} - \vartheta_i^{(n)}}{\delta_t} + \frac{\delta}{\delta_t} \frac{\vartheta_{i+1}^{(n+1)} - \vartheta_i^{(n+1)}}{\delta}$$

and a first-order-accurate explicit Euler discretization for the collision part, $\Omega_a^{(n)}$ [94]. This results in the “basic” two-step “stream-and-collide” LBE algorithm¹¹ (see Algorithm I).

3.2. Advanced Numerical Schemes

3.2.1. Numerical discretization of the advection operator

Let’s consider general three-point finite-difference formula for discretization of eq.(31), at point i in “ a^{th} ” direction of the particle’s motion¹²:

$$\vartheta_i^{n+1} = a_i \vartheta_{i-1}^\diamond + b_i \vartheta_i^\diamond + c_i \vartheta_{i+1}^\diamond + \Omega_i^\diamond \quad (32)$$

The upper indices denote the level of implicitity: $\diamond = n$ (explicit), $\diamond = n + 1/2$ (semi-implicit), and $\diamond = n + 1$ (implicit). Eq.(32) can be written in the following “conservative” form, [76]:

$$\begin{aligned} \vartheta_i^{n+1} = \vartheta_i^n - \frac{1}{2} \left[\text{CFL}_{i+\frac{1}{2}} (\vartheta_{i+1}^\diamond + \vartheta_i^\diamond) - \text{CFL}_{i-\frac{1}{2}} (\vartheta_i^\diamond + \vartheta_{i-1}^\diamond) \right] + \\ + \left[\nu_{i+\frac{1}{2}}^{(\text{n.d.})} (\vartheta_{i+1}^\diamond - \vartheta_i^\diamond) - \nu_{i-\frac{1}{2}}^{(\text{n.d.})} (\vartheta_i^\diamond - \vartheta_{i-1}^\diamond) \right] + \Omega_i^\diamond \end{aligned} \quad (33)$$

where $\nu_{i \pm \frac{1}{2}}^{(\text{n.d.})}$ are the dimensionless coefficients of numerical diffusion, and

$$\begin{aligned} a_i &\equiv \nu_{i-\frac{1}{2}}^{(\text{n.d.})} + \frac{1}{2} \text{CFL}_{i-\frac{1}{2}} \\ b_i &\equiv 1 - \frac{1}{2} \text{CFL}_{i+\frac{1}{2}} + \frac{1}{2} \text{CFL}_{i-\frac{1}{2}} - \nu_{i+\frac{1}{2}}^{(\text{n.d.})} - \nu_{i-\frac{1}{2}}^{(\text{n.d.})} \\ c_i &\equiv \nu_{i+\frac{1}{2}}^{(\text{n.d.})} - \frac{1}{2} \text{CFL}_{i+\frac{1}{2}} \end{aligned} \quad (34)$$

Application of eqs.(32)-(34) to the ‘stream-and-collide’ equations (29-30) gives $\nu^{(\text{n.d.})} = 1/2$, [94]. This numerical diffusion can be compensated for by modifying the relaxation

¹¹It is instructive to note that with chosen notation $f_a(\mathbf{x} + \mathbf{e}_a \delta_t, t + \delta_t) = \vartheta_{i+1}^{(n+1)}$.

¹²It is instructive to note that, in the present section, “ i ” is a point of the finite-difference discretization of eq.(31), discretized in the a^{th} -direction.

parameter from τ^* to $(\tau^* - 1/2)$.

For the “stream-and-collide” scheme, the “Courant, Friedrichs, and Lewy” number for advection is $\text{CFL} = \frac{\varepsilon_a \delta t}{\Delta x_a} \equiv 1$. This condition $\text{CFL}=1$ is quite restrictive, especially in the case of the strong non-linearity of the collision operator¹³. The following ‘predictor-corrector’ algorithm has been introduced in [74], allowing to overcome this problem.

**A
L
G
O
R
I
T
H
M**

“Multifractional stepping procedure (MF \mathbb{N})”:

In this scheme, a time step from n to $n + 1$ is divided in to $2\mathbb{N}$ sub-steps.

The downwind/upwind difference are employed for an advection term, at each odd/even sub-step:

$$\begin{aligned} \vartheta_i^{(2m+1)} &= \vartheta_i^{(2m)} + \frac{\vartheta_i^{(2m)} - \vartheta_{i+1}^{(2m)}}{2^{[\mathbb{N}]}} + \frac{\Omega_i \diamond}{2^{[\mathbb{N}]}} \\ \vartheta_i^{(2m+2)} &= \vartheta_i^{(2m+1)} + \frac{\vartheta_{i-1}^{(2m+1)} - \vartheta_i^{(2m+1)}}{2^{[\mathbb{N}]}} + \frac{\Omega_i \diamond}{2^{[\mathbb{N}]}} \end{aligned} \quad (35)$$

$m = 0, \dots, (\mathbb{N} - 1)$

With this scheme, the CFL number can be varied arbitrarily, $\text{CFL} = \frac{1}{2\mathbb{N}}$. For $\mathbb{N} = 1$, this scheme is identical to the explicit MacCormack scheme [76]. Furthermore, for each couple of sub-steps, the central differencing is applied in both time and space, rendering thus the second-order accuracy. Applying eqs.(32)-(34), the sub-step coefficient of the numerical diffusion is $\nu^{(\text{n.d.})} = -\frac{1}{4\mathbb{N}}$ for odd sub-steps, and $\nu^{(\text{n.d.})} = +\frac{1}{4\mathbb{N}}$ for even sub-steps. Thus, the resulting coefficient of the numerical diffusion is zero.

Other algorithms for discretization of the LBE’s advection operator were also proposed to help alleviating a stability problem in the LBE numerical treatment; see [98] (“TVD/AC” scheme) and [71] (“Lax-Wendroff” scheme). The stability problem is even more acute in the simulation of multiphase and thermal flows ([74], [98], [71]).

3.2.2. Numerical discretization of the collision operator

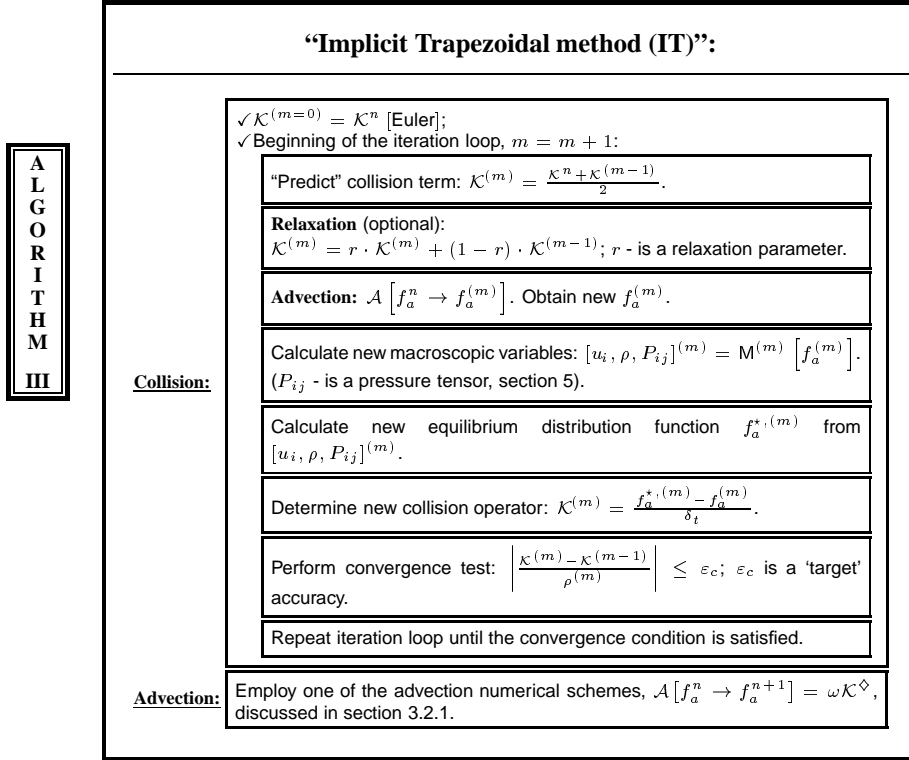
The ‘stream-and-collide’ LBE numerical scheme employs the explicit Euler method for the collision operator. In the case of $\omega = \frac{1}{\tau^*} \rightarrow 2$, and in the case of the strong non-linearity of the collision operator, this scheme fails to produce stable solutions [94] [74]. Notice, that the LBE equations (31)

$$\frac{\mathcal{A}(f_a)}{\omega} \equiv \underbrace{D_\omega f_a}_{\mathcal{K}} \equiv \frac{f_a^{\text{eq}} - f_a}{\delta t} \quad (36)$$

¹³For example, in the case of the complex fluids, section 4.

are stiff differential equations in ω : $f_a \sim e^{\sim \omega}$. This means, that an error would grow exponentially.

Several numerical schemes were developed for the solution of stiff differential equations (see for review [76]). For example, the first- and the second-order explicit Runge-Kutta methods can be used to reduce the error growth, [74]. It is instructive to note that the Runge-Kutta schemes do not guarantee stability for the stiff equations. To address this problem, Nourgaliev et al. developed an *implicit trapezoidal method* (IT) [74] (Algorithm III).



Stability of the IT algorithm is achieved by means of an iterative formulation of the collision operator

$$D_\omega f_a = \frac{\mathcal{K}^n + \mathcal{K}^{n+1}}{2} \quad (37)$$

This scheme is second-order accurate, $O(\omega^2)$. Also, from the Von Neumann linear stability analysis, it can be shown that IT scheme is A-stable (absolute stability in the entire left half-plane, [76]). However, the IT scheme is iterative. The iterations converge rapidly, especially when the ‘MFN’ scheme is employed for an advection. In addition, the convergence rate increases with the increase of the number of sub-steps N , [74]. This feature is of importance for simulations of high-surface-tension and high-density-ratio non-ideal fluids [74].

3.3. Remarks on the LBE numerical implementation

Time step and lattice size. In the LBE simulations, the dimensionless relaxation parameter (see eq.(5)):

$$\tau^* \equiv \frac{\varepsilon \hat{\tau}}{\hat{\delta}_t} = \frac{\tau}{\delta_t} \quad (38)$$

is typically in the range $\frac{1}{2} < \tau^* < 3$, where the lower limit is dictated by the consideration of the numerical stability of the scheme. As it will be seen later in section 5.2, the kinematic viscosity is¹⁴

$$\nu = \tau^* \delta_t c_s^2; \quad \text{or} \quad \nu = \underbrace{\left(\tau^* - \frac{1}{2} \right) \delta_t c_s^2}_{\text{“stream-and-collide”}} \quad (39)$$

From eq.(39), it is seen that in order to model fluid with specific kinematic viscosity (say, water or air) for a chosen spatial discretization δ_x and relaxation parameter τ^* , one has to fix a time step of the LBE simulation. For example, in the case of the D_2Q_9 “stream-and-collide” scheme with $w_0 = \frac{4}{9}$, time step is

$$\delta_t = \frac{(\tau^* - \frac{1}{2}) \delta_x^2}{3\nu}; \quad \hat{\delta}_t = \frac{(\tau^* - \frac{1}{2}) \hat{\delta}_x^2 \text{Re}}{3} \quad (40)$$

Setting the range of the kinematic viscosity from $10^{-7} \frac{m^2}{s}$ (water) to $10^{-3} \frac{m^2}{s}$ (highly viscous oils), simulation using the space resolution $\delta_x = 1\text{mm}$ and relaxation parameter $(\tau^* - \frac{1}{2}) \sim 1$ would require the following range of time step: δ_t varying from $\frac{1}{3} \cdot 10\text{s}$ to $\frac{1}{3} \cdot 10^{-3}\text{s}$. It is interesting to compare these estimates with the “viscous” CFL (“Courant-Friedrichs-Levy”) limit of the explicit schemes of the “continuum” CFD, $\delta_t = \text{CFL}_{\text{vis}} \frac{\delta_x^2}{\nu} \sim \text{CFL}_{\text{vis}} (10 \div 10^{-3}) s$. From this, one can make the following observations. First, the “viscous CFL number” of the LBE is $\text{CFL}_{\text{vis}}^{(\text{LBE})} = (\tau^* - \frac{1}{2}) \frac{c_s^2}{c^2} = \frac{\tau^* - \frac{1}{2}}{3} \Big|_{D_2Q_9}$. Next, for $\tau^* > 3.5$, the D_2Q_9 LBE method allows to utilize larger time step than the one admissible for explicit “continuum CFD” schemes, $\text{CFL}_{\text{vis}}^{(\text{LBE})} > 1$. However, for small relaxation parameter, $\tau^* \rightarrow \frac{1}{2}$, time step of the LBE becomes too small, $\text{CFL}_{\text{vis}} \ll 1$. As seen from eq.(40), in order to increase the Re number for a chosen discretization $\hat{\delta}_x$ and $\hat{\delta}_t$, one needs to decrease the relaxation time $\tau^* \rightarrow \frac{1}{2}$. This causes two problems. First, the dimensional time step δ_t decreases according to eq.(40); and, second, the “stream-and-collide” LBE BGK schemes become unstable¹⁵ when $\tau^* \approx \frac{1}{2}$, [94]. An alternative approach to increase the Re number (while keeping sufficiently large δ_t and τ^* within the stability range), is to decrease the non-dimensional lattice step $\hat{\delta}_x \sim \frac{1}{N}$ by increasing the number of computational nodes N . This makes the LBE simulations of high-Re-number flows computationally expensive.

¹⁴In the case of the “stream-and-collide” scheme (see section 3.1), there is a numerical-diffusion-related viscosity coefficient absorbed into ν by modifying $\tau^* \rightarrow (\tau^* - \frac{1}{2})$. This coefficient is due to the first-order accuracy of the advection operator with the expansion eq.(62), [94].

¹⁵Development of new (non-BGK) LBE schemes is promising, from the scheme stability point of view [60].

Requirements for acoustics. Simulation of compressible fluid flows using the isothermal LBGK model is not practical. To adequately represent the sound speed in air ($c_s|_{T=300K} = \sqrt{\gamma RT} \approx 300 \frac{m}{s}$ and $\nu_{air} \approx 10^{-5} \frac{m^2}{s}$), considered as an ideal gas, a time step $\delta_t = \frac{\nu}{(\tau^* - \frac{1}{2})c_s^2} \approx 10^{-8}s$ would be required for the D_2Q_9 “stream-and-collide” LBGK scheme (with $(\tau^* - \frac{1}{2}) = 10^{-2}$ to ensure the numerical stability). The corresponding grid size is $\delta_x = \sqrt{3}c_s\delta_t \approx 1\mu m$. Similar estimates for water¹⁶ ($c_s \approx 1500 \frac{m}{s}$ and $\nu_{H_2O} \approx 10^{-7} \frac{m^2}{s}$) yield $\delta_t \approx 10^{-11}s$ and $\delta_x \approx 10nm$.

Direct counterpart of the LBE method in “traditional” CFD is the Chorin’s method of artificial compressibility [20]. In this approach, the governing equations of viscous incompressible fluid dynamics are substituted by the following system of equation:

$$\text{The method of Artificial Compressibility (AC)} \quad \begin{cases} \partial_t \rho + \partial_j \rho_{ref} u_j = 0 \\ \partial_t u_i + \partial_j u_i u_j = -\frac{\partial_i P}{\rho_{ref}} + \nu \partial_j (\partial_i u_i + \partial_i u_j) + g_i \\ P = \frac{\rho}{\delta} : \text{Artificial equation of state} \end{cases} \quad (41)$$

Remark 3:

where ρ_{ref} is the density of the modeled incompressible fluid; ρ is the *artificial density*; $\delta = \frac{1}{\sqrt{c_s}}$ is the *artificial compressibility*; and c_s is the *artificial sound speed*. One can also introduce the *artificial Mach number*, defined as $M = \frac{U_0}{c_s}$, where U_0 is a characteristic velocity scale. As can be seen later (section 5.2), this set of governing equations is essentially the same as that of the LBE method, except that there are no artifact terms present and there exist a greater flexibility to vary fluid viscosity. Recent development of the Chorin’s AC method is a “Numerical Acoustic Relaxation” (NAR) method, [75]. In [75], one can find more about comparison of the LBE and NAR.

4. LATTICE BOLTZMANN MODELS FOR HYDRODYNAMICS OF COMPLEX FLUIDS

In the present section, a comprehensive review and critical analysis of all major LBE-based methods for modeling of complex fluid behavior are presented. We start with general remarks on the “LBE hydrodynamics”, section 4.1. Then, most commonly used LBE models for complex fluids are described in sections 4.2-4.6. Finally, “pros” and “cons” of the LBE modeling framework for simulation of multiphase flows and complex fluids are discussed in details in section 4.7.

4.1. General remarks

Modeling of incompressible fluids. As it can be seen from the discussion in section 3.3, due to severe limitations on time step and grid size, the LBE method is practically limited to the modeling of incompressible low-Re-number fluids.

Modeling of thermal flows. Modeling of the ‘complete’ set of transport equations (mass, momentum, energy) using the discrete kinetic approach has met with significant difficulties. There are three major ‘plagues’ of the LBGK thermohydrodynamics. *First*, the thermal LBGK models are limited to $Pr = \frac{1}{2}$ due to a single relaxation time [3]. *Second*, the thermal LBGK models have severe limitations on allowable variations of temperature

¹⁶Importantly, water cannot be considered as an “ideal gas” due to the “stiff” pressure-density relation, $P \sim \rho^{7.15}$.

and velocity due to the limited set of the discrete particle velocities. *Third*, the ‘thermal’ LBGK models are prone to numerical instabilities due to ‘large stencil’ of discrete velocities, required to recover correct macroscopic equations; [50] [10] [71] [95] [72] [36]. For these reasons, the thermal LBGK models were found inferior to a “continuum CFD” finite-difference methods ([72]) in computational time, memory requirement and stability. In practice, energy transport and phase transition cannot be modeled with the existing LBE models and technology¹⁷. Thereafter, we will limit our consideration to the “isothermal” LBE models.

Modeling of thermodynamic behavior. Several LBE models were developed to account for “non-ideality”, external forcing, and different phenomena associated with intermolecular interactions. Extension of the LBE method to nonuniform (non-ideal) gases, and more generally to fluid-fluid multiphase flows, is accomplished either heuristically (by applying certain rules which “mimic” complex-fluid behaviour); or based on the Enskog’s extension of the Boltzmann’s theory to dense gases, with incorporation of the phenomenological models of quasilocal equilibrium constant-temperature thermodynamics; and using the LBE methodology to couple the later one to the hydrodynamics of complex fluid. The major challenge is to accurately describe the physical mechanisms that govern the interface evolution (transport, breakup and coalescence). The chief difficulty is related to the breakdown of the continuum mechanics theory at the fluid interfaces, where material properties experience drastic changes. Considering interfaces, one naturally and intuitively thinks in terms of molecules of different kind, interacting over very short distance across the interfaces. Thus, intuitively, the models operating with the concept of particles and molecules should have methodological advantages over the methods of the ‘continuum mechanics’.

Modeling of particulate suspensions in incompressible fluids. The LBE method has been successfully applied to particulate suspensions in incompressible fluids, a class of problems with complex geometry and moving boundaries. The key here is to accurately account for the momentum transfer across the solid-fluid boundary while conserving mass. In general, there are two basic LBE formulations ([58],[59], [1] and [2]) for this class of problems.

In the first approach ([58] and [59]), the fluid occupies the entire computational domain with the solid particles occupied with ‘interior’ fluid, eliminating the solid-fluid interface as far as mass conservation is concerned. This approach gives accurate results as long as the time scale based on the kinematic viscosity of the interior fluid is sufficiently small and the contribution of the inertia of the interior fluid is accounted for when computing the inertia of the particle. This formulation can be used only when the solid density is larger than the fluid density.

The second approach ([1] and [2]) considers the solid particle without the interior fluid and, therefore, applies to any solid to fluid density ratio. The LBE based simulations of suspended particles give results [2] in good agreement with the finite element solutions of the Navier-Stokes equations [30] for low to moderate particle Reynolds number. It is

¹⁷Recent studies of non-BGK LBE & implicit LBE models might lead to the progress in this direction [60].

shown [23] that this method, when applied with care, can produce very accurate particle trajectories over very long time periods, making it possible to investigate the dynamics and stability of particle motion, even near points of bifurcation. By analysis of the appropriate phase-space trajectories near transition points, the LBE method has been useful in revealing the type of bifurcation and the scaling laws governing the particle motion [23].

4.2. Enskog extension to dense gases

In real ('dense', 'non-ideal') gases, the mean free path is comparable with molecular dimensions. Thus, additional mechanisms for momentum and energy transfer must be considered. Beside the transfer of molecular properties *between* collisions, a transfer *during* the collision events must be accounted for [15]. This collisional transfer has been considered by Enskog (1921) [27], who approximated the effect of the exclusion volume of the molecules under constant temperature conditions by explicitly adding the 'exclusion volume' term into the Boltzmann collision integral. The most commonly used (approximate) form of this term is

$$(\partial_t f)_{\text{coll, Enskog}} = (\partial_t f)_{\text{coll, Boltzmann}} - \underbrace{f^{\text{eq}} b \rho \chi (\mathbf{e} - \mathbf{u}) \cdot \nabla \ln(\rho^2 \chi)}_{\substack{\text{Approximation of} \\ \text{the Enskog's} \\ \text{'exclusion volume'} \\ \text{term}}} \quad (42)$$

where $b = \frac{2\pi d}{3m}$ is the second virial coefficient in the virial equation of state; χ is the increase in collision probability due to the increase in fluid density, which has the following asymptotic form [15]:

$$\chi = 1 + \frac{5}{8} b \rho + 0.2869 (b \rho)^2 + 0.1103 (b \rho)^3 + \dots \quad (43)$$

and d and m are the diameter and mass of the molecules, respectively. Combination of eqs.(1), (2) and (42), known as the 'Enskog equation' in the literature [39], was adopted by Luo in an attempt to develop a 'unified theory of lattice Boltzmann models for nonideal gases'¹⁸, [66].

It is instructive to note that, in his derivation, Enskog employed a 'hard-sphere model', which has the advantage of mathematical simplicity, since many-body interactions are neglected (collisions are instantaneous). This model is, however, not appropriate for real gases under high pressure, because the molecules are in the force field of others during a large part of their motion, and multiple encounters are not rare¹⁹, [15].

¹⁸Luo employed the BGK collision operator multiplied by χ , $(\partial_t f)_{\text{coll, Boltzmann}} = -\frac{\chi(f - f^{\text{eq}})}{\tau}$.

¹⁹Enskog's preference of the 'hard-sphere model' rooted in the belief that molecular chaos is valid for rigid spherical molecules even at high gas densities. This assumption is accurate only for uniform steady state [15], while for non-uniform state (for example, in the regions of fluid-solid boundaries and fluid-gas interfaces), correlation between velocities of neighboring molecules may exist due to a memory effect.

4.3. He, Shan and Doolen extension to dense gases

He, Shan and Doolen (1998) [44] proposed the following approximate model of dense gases. The starting point was the LBGK equation in the form²⁰:

$$\partial_t f + \mathbf{e} \cdot \nabla_{\mathbf{r}} f = -\frac{f - f^{\text{eq}}}{\tau} + \frac{(\mathbf{F} + \mathbf{g}) \cdot (\mathbf{e} - \mathbf{u})}{\rho c_s^2} f^{\text{eq}} \quad (44)$$

where \mathbf{F} and \mathbf{g} are the effective molecular interaction and gravity forces, respectively, $\mathbf{a} = \frac{\mathbf{F} + \mathbf{g}}{\rho}$. The effective molecular interaction force \mathbf{F} is designed to simulate non-ideal gas effects.

$$\mathbf{F} = \underbrace{-\rho \nabla \mathcal{V}}_{\text{Intermolecular attraction by mean-field approximation}} - \underbrace{\mathbf{b} \rho^2 c_s^2 \chi \cdot \nabla \ln(\rho^2 \chi)}_{\text{Enskog's exclusion volume effect of the molecules on the equilibrium properties of dense gases}} \quad (45)$$

The intermolecular attraction potential²¹ \mathcal{V} is expressed as

$$\mathcal{V}(\mathbf{r}_0) = \int_{r_{01} > d} u_{\text{attr}}(r_{01}) \rho(\mathbf{r}_1) d\mathbf{r}_1 \quad (46)$$

where $u_{\text{attr}}(r_{01})$ is the attractive component of the intermolecular pairwise potential of molecules '0' and '1' separated by distance $r_{01} = |\mathbf{r}_0 - \mathbf{r}_1|$. The next step is to expand density about \mathbf{r}_0 . Assuming that density gradients are small, the intermolecular attraction potential is expressed as

$$\mathcal{V} = -2a\rho - \kappa \nabla^2 \rho \quad (47)$$

where constants a and κ are given by

$$a = -\frac{1}{2} \int_{r>d} u_{\text{attr}}(r) d\mathbf{r}; \quad \kappa = -\frac{1}{6} \int_{r>d} r^2 u_{\text{attr}}(r) d\mathbf{r} \quad (48)$$

with κ determining the strength of the surface tension. Elucidating the thermodynamical aspects of this model, the intermolecular force \mathbf{F} can be cast into the following form [40]:

$$\mathbf{F} = -\nabla P^* + \underbrace{\kappa \rho \nabla \nabla^2 \rho}_{\text{Force associated with surface tension}} \quad (49)$$

$$P^*(\rho) = \mathbf{b} \rho^2 c_s^2 \chi - a \rho^2 = \underbrace{P - \rho c_s^2}_{\text{'Non-ideal part' of the equation of state}}; \quad P = \rho c_s^2 (1 + \mathbf{b} \rho \chi) - a \rho^2$$

²⁰Here, we would like again to note the conceptual difficulty with interpretation of the "LBE's molecules", due to the definition of sound speed by eq.(14) (see Remark 1).

²¹Implementation of the intermolecular attraction potential \mathcal{V} allows to effectively compensate for certain limitations of the Enskog 'hard-sphere' model.

Setting $b = \frac{\chi-1}{\rho\chi}$, the van der Waals equation of state is obtained²²:

$$P = \frac{\rho c_s^2}{1 - b\rho} - a\rho^2 \quad (50)$$

4.4. Free-energy-based models

Swift et al. ([96] and [97]) developed a model for non-ideal fluids to account for the interfacial thermodynamics. The general idea is to incorporate phenomenological approaches of interface dynamics, such as Cahn-Hilliard and Ginzburg-Landau models, using the concepts of free-energy functional; and to utilize the discrete kinetic approach as a vehicle for coupling with complex-fluid hydrodynamics. The pressure tensor is defined using the Cahn-Hilliard's approach for non-equilibrium thermodynamics. Strictly speaking, this model is phenomenological, in which the thermodynamic effects are introduced through a *phenomenological equation of state*. The term 'free-energy-based' is attributed to the model chosen for pressure tensor eq.(51) [13].

$$\mathcal{P}_{i,j}^{(0)} = \left[P_0 - \kappa \rho \partial_k^2 \rho - \frac{\kappa}{2} (\partial_k \rho)^2 \right] \delta_{i,j} + \kappa \partial_i \rho \cdot \partial_j \rho \quad (51)$$

Thermodynamical pressure P_0 can be given by, e.g., van der Waals equation, eq.(50). Parameter κ is a measure of the interface free energy. For flat interfaces, κ is related to the coefficient of surface tension σ through the equation:

$$\kappa = \frac{\sigma}{\int \left(\frac{\partial \rho}{\partial n} \right)^2 dn} \quad (52)$$

where n is the normal-to-interface direction.

Multi-component versions of the free-energy-based model were developed in [97] and [62].

4.5. Interparticle interaction potential model of Shan and Chen

One of the first LBE model for multiphase flow is due to Shan and Chen [90] [91] [92] [93]. In this model, an additional momentum forcing term is explicitly added to the velocity field after each time step:

$$\begin{aligned} \mathbf{u}'(\mathbf{x}, t) &= \mathbf{u}(\mathbf{x}, t) + \vec{\Gamma}(\mathbf{x}, t) \quad \text{where} \\ \vec{\Gamma}(\mathbf{x}, t) &= -\frac{\tau}{\rho} \psi(\mathbf{x}) \sum_a^b \mathcal{G}_a \psi(\mathbf{x} + \mathbf{e}_a) \mathbf{e}_a \end{aligned} \quad (53)$$

where ψ is a "potential" function and \mathcal{G} is a "strength" of the interparticle interaction. The 'corrected' velocity \mathbf{u}' is employed in the equilibrium distribution function, given by eq.(B.9). By introducing an additional forcing term, this model *effectively mimics* the

²²Other equations of state can be implemented in a similar way.

intermolecular interactions ('complex fluid behaviour'). Although it is possible to show that the total momentum in the whole computational domain is conserved [91], the momentum is not conserved locally. As a result, a spurious velocity always exists in regions adjacent to the interface, Fig. 2. The forcing term $\vec{\Gamma}$ in eq.(53) corresponds to the following non-local potential function

$$\mathcal{V}(\mathbf{x}, \mathbf{x}') = \mathcal{G}(\mathbf{x}, \mathbf{x}') \psi(\mathbf{x}) \psi(\mathbf{x}') \quad (54)$$

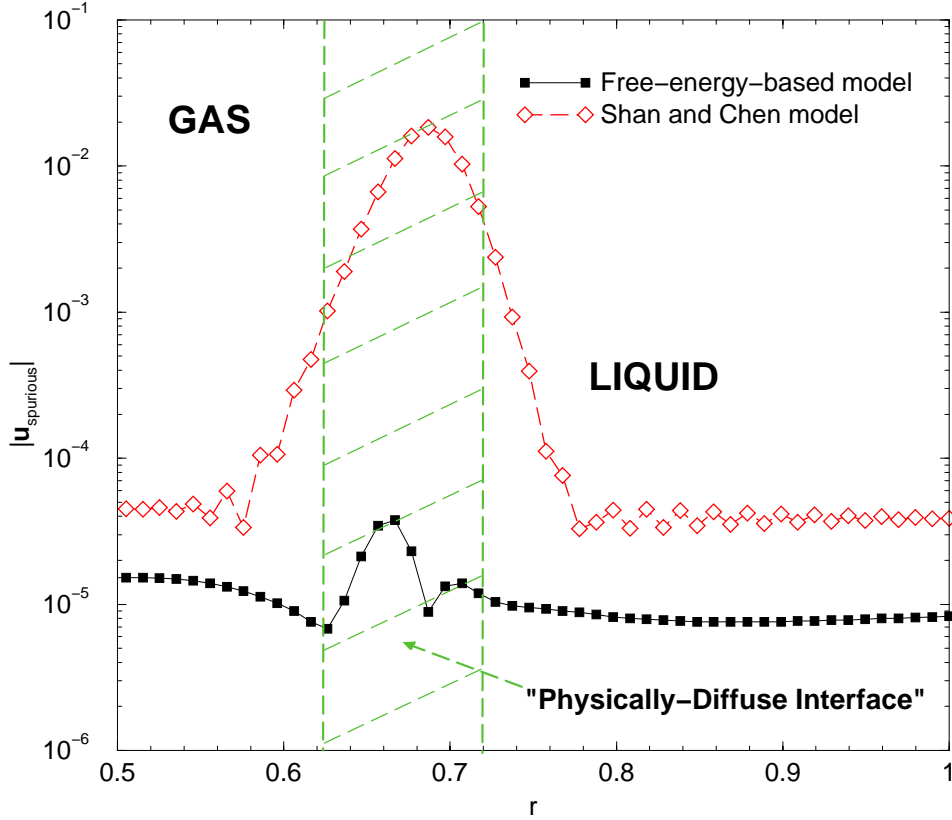


FIG. 2. Velocity distribution across the interface for the “Shan-Chen” and “Free-energy-based” models. Bubble of the van der Waals fluid at equilibrium, [74].

One can avoid the step eq.(53) by directly substituting \mathbf{u}' into the equilibrium distribution function eq.(B.9). Effectively, this means addition of the following “correction” term to the equilibrium distribution function [74]:

$$\begin{aligned} f_a^{\text{eq}} &= f_a^{\text{eq}} + \delta f_a^*, \quad a = 0, \dots, b \\ \delta f_0^* &= \left[\frac{1 - w_0}{\Upsilon^{(2)}} - \frac{\Upsilon^{(2)}}{\Upsilon^{(4)}} \right] \cdot \left[\Gamma_i u_i + \frac{\Gamma_i^2}{2\rho} \right] \quad \text{and} \\ \delta f_{a \neq 0}^* &= w_a \left[\frac{e_{a_i} \Gamma_i - u_i \Gamma_i - \Gamma_i^2 / (2\rho)}{\Upsilon^{(2)}} + \frac{e_{a_i} e_{a_j}}{2\Upsilon^{(4)}} \left\{ \Gamma_i u_j + \Gamma_j u_i + \frac{\Gamma_i \Gamma_j}{\rho} \right\} \right] \end{aligned} \quad (55)$$

4.6. He, Chen and Zhang model

He et al. (1999) [40] extended the HSD model to incompressible multiphase flow. Two sets of distribution function are utilized. The first one is used to “capture” incompressible fluid’s pressure and velocity fields, using the concept of “artificial compressibility” [41]. Another discrete distribution function i_a is introduced with the sole purpose to “capture” the interface; which makes this approach close in spirit to the “continuum CFD” methods for interface capturing - the “level set” and “volume-of-fluid” approaches. After each time step, the “index” function $\phi = \sum_a i_a$ is re-constructed, allowing to enforce a smooth transition of densities and viscosities at the “numerically smeared” interface:

$$\begin{aligned}\rho(\phi) &= \rho_1 + \frac{\phi - \phi_1}{\phi_2 - \phi_1} (\rho_2 - \rho_1) \\ \nu(\phi) &= \nu_1 + \frac{\phi - \phi_1}{\phi_2 - \phi_1} (\nu_2 - \nu_1)\end{aligned}\tag{56}$$

where ρ_1, ρ_2, ν_1 and ν_2 are density and kinematic viscosity of the two fluids; and ϕ_1, ϕ_2 are the minimum and maximum values of the ‘index’ function, respectively.

4.7. Assessment of the LBE modeling framework for multiphase flow and complex fluids

Since the lattice Boltzmann equation method is a *particle method*, it is argued that, for simulation of interfacial phenomena, the LBE method has potential to be superior comparing to the “continuum” CFD methods [90] [91] [92] [93] [96] [97] [102]. In the present section, we will address the question whether, why and when the LBE approach may be advantageous for simulation of the interfacial phenomena. It is important to realize that the computational modeling of multiphase flows is not open for ‘purism’. That is, there are no ‘universal models’ able to perfectly work under any flow conditions. One has to be aware of the limitations and advantages of the approach chosen, since every one has its own domain of applicability. In Appendix C, we provide a classification of the modern computational methods for fluid-fluid multiphase flows, which would enable us to properly appreciate the perspectives of the discrete kinetic approach.

To discuss the LBE method for multiphase flows, we have chosen three most successful and popular LBE models: the ‘Shan-Chen’ (‘SC’) model (section 4.7.1); the ‘free-energy-based’ model (section 4.7.2); and the ‘He-Shan-Doolen’ (‘HSD’) model (section 4.7.3). The other multiphase LBE models are due to Gunsteinsten et al. [38] and Luo [66].

4.7.1. ‘Shan-Chen model

The ‘SC’ LBE method [90] [91] [92] [93] has been quite successful in simulation of several fundamental interfacial phenomena, such as, e.g., Laplace law for static droplets/bubbles and oscillation of a capillary wave (see for review [16]). However, there are a few limitations of the ‘SC’ model, which make this method inferior in comparison to other methods for multiphase flows.

- The first serious problem is that one cannot introduce temperature which is consistent with thermodynamics. It is possible to show that the ‘SC’ model has the following equation

of state [91]:

$$P = c_s^2 \rho + \underbrace{\frac{bc^2 \mathcal{G}}{2D} \psi^2(\rho)}_{P^*} \quad (57)$$

where $b = 24$ and $D = 2$ for a D_2Q_9 lattice. Suppose we would like to study fluid with the ‘non-ideal’ part of the equation of state P^* . In order to reproduce this equation of state, the following ψ function must be utilized:

$$\psi(\rho) = \sqrt{\frac{2DP^*}{bc^2 \mathcal{G}}}; \quad P^* = P - c_s^2 \rho \quad (58)$$

It is possible to show, that the Maxwell’s “equal-area” reconstruction is possible only for one special form of the potential function, $\psi = \psi_0 \exp(-\rho_0/\rho)$, where ψ_0 and ρ_0 are arbitrary constants [91]. The role of temperature in this model is effectively taken by the strength of the interparticle interactions \mathcal{G} . By varying \mathcal{G} , one could construct $(\mathcal{G} - \rho)$ -diagram, which mimics the $(T - \rho)$ -diagram, Fig. 3.

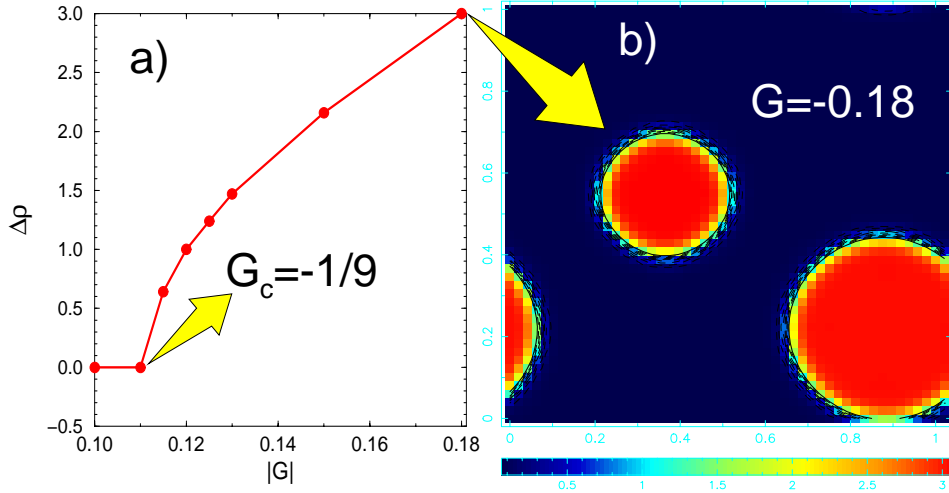


FIG. 3. a) $(\mathcal{G} - \Delta\rho)$ -diagram for the ‘SC’ model ($\Delta\rho = \rho_{\text{liq}} - \rho_{\text{gas}}$), demonstrating the occurrence of the first-order phase transition at the analytically predicted “critical” strength of interparticle interactions, $\mathcal{G} = \frac{1}{9}$, [86]. b) Typical density distribution at the state, close to the equilibrium.

- The next problem is related to the way this model represents capillary effects, which can be quantified by the coefficient of surface tension σ . It can be shown, that for the ‘SC’ model, in the case of the flat interface, the coefficient of surface tension can be calculated from the following equation [91]:

$$\sigma = \frac{c^2}{D+2} \int_{-\infty}^{+\infty} \sqrt{P^*} \cdot \frac{d^2 \sqrt{P^*}}{dn^2} dn \quad (59)$$

where n is a direction normal to the interface. This means that σ is coupled to the equation of state through P^* and there is no freedom to vary it. Typically, for a chosen potential function and “strength of interparticle interactions \mathcal{G} ”, the surface tension of the “SC” model is “empirically” determined by generating circular bubbles/droplets of different radii in a

periodic domain, and estimating the slope of the “pressure-difference vs. inverse of radius” relation (Laplace law, Fig.4), [104], [86].

- Another severe limitation is related to the inability to represent different viscosities in different phases. All LBE simulations of multiphase flows performed *to date* have assumed that all phases or components of the multiphase system possess the same kinematic (ν) and “second” ($\frac{\xi}{\rho}$) viscosities, defined by the relaxation time²³ τ and lattice geometry, eq.(84).

In our classification of the CFD methods for multiphase flows, Appendix C, the ‘SC’ model belongs to the class of “physically-diffuse-interface” methods. These methods do not require to “track” or “capture” the interface position, since the “phase separation” and “interface sharpening” mechanisms are provided by the momentum forcing term $\vec{\Gamma}$. Effectively, $\vec{\Gamma}$ plays the role of both the Korteweg’s capillary stress tensor and the “non-ideal” part of the equation of state P^* . The ‘SC’ method builds the interface physical model based on the continuum variable ρ : $\vec{\Gamma} = \mathcal{F}[\psi = f(\rho)]$. There is no direct use of the one-particle probability distribution function, f_a - a distinct feature of the LBE method.

4.7.2. “Free-energy-based” model by Swift *et al.*

The free-energy-based LBE approach has been applied to several physical phenomena in binary and ternary fluids, such as flow patterns in lamellar fluids subjected to shear flow [34]; effect of shear on droplet phase in binary mixtures [102]; spontaneous emulsification of droplet phase in ternary fluid, which mimics the oil-water-surfactant systems [62]; etc.

The main advantage of this model over the ‘SC’ LBE method is that it was formulated to account for equilibrium thermodynamics of non-ideal and multi-component fluids at a fixed temperature, allowing thus to introduce well-defined temperature and thermodynamics. The model is, therefore, consistent with the “Maxwell’s equal-area reconstruction” procedure, Fig.5.

Furthermore, since the model admits local momentum conservation, the interfacial spurious velocity is nearly eliminated [74], Fig.2.

Similar to the ‘SC’ model, the free-energy-based models do not utilize the ‘particle’ nature of the discrete kinetic approach. The major drawback of this approach is that the model suffers from unphysical Galilean invariance effects, coming from the ‘non-Navier-Stokes’ terms, which appear at the level of the Chapman-Enskog analysis of the discrete Boltzmann equation (see section 5.4 and Appendix E). Efforts are being made to reduce this unphysical effect [48].

²³One possible way to vary viscosity is to introduce spatially-variable relaxation time, which allows variable viscosity in the ‘bulk’ region of different fluids [67]. Effect of this approach on dynamics of interface has yet to be investigated.

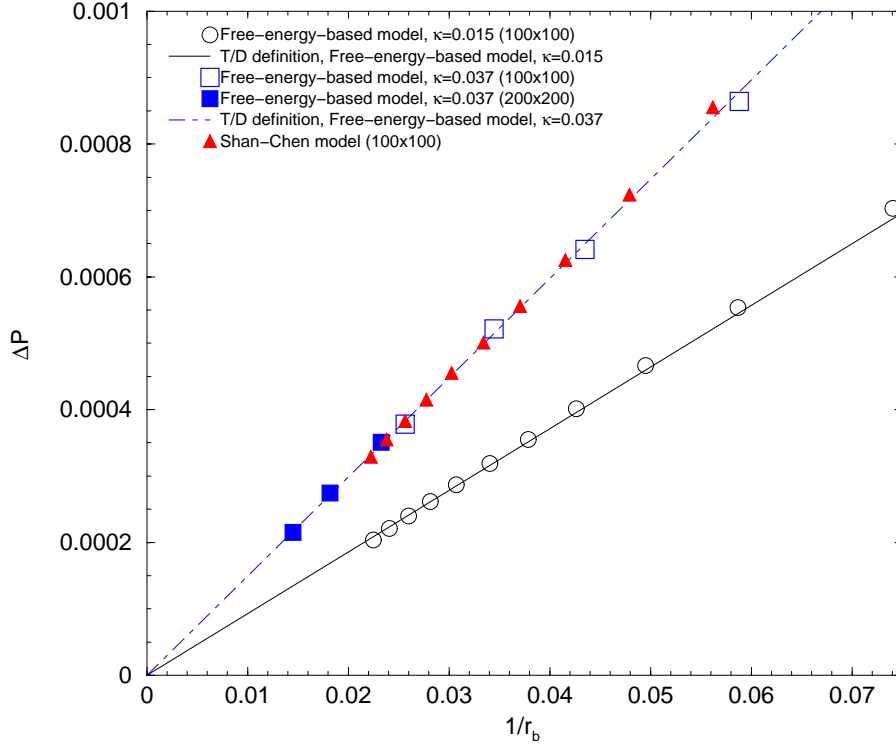


FIG. 4. Laplace law for the “SC” and the “free-energy-based” models: ΔP as a function of $\frac{1}{r_b}$ (r_b is a radius of the generated bubble) for a van der Waals fluid. Solid and dashed lines are the results from the “flat interface test”, with thermodynamical definition of surface tension by eq.(52), [74].

4.7.3. He, Shan and Doolen model

This model was developed [44] as a revision of the ‘SC’ model. In difference to the ‘SC’ model, the ‘HSD’ model is linked to the kinetic theory of dense gases, section 2.1. The intermolecular interactions are formulated using the approximation of the Enskog extension of the Boltzmann equation. As a result, the ‘HSD’ approach is more flexible for implementation of the thermodynamical model, with the “consistent” temperature concept, admitting the correct Maxwell’s “equal-area” reconstruction procedure. The capillary effects are modeled by the explicit implementation of the “density gradient model”, $\kappa \nabla^2 \rho$, eq.(49), allowing flexibility in variation of the coefficient of surface tension by varying the parameter κ .

The serious limitation of the “HSD” model is related to the numerical instability, associated with the ‘stiffness’ of the collision operator, when the ‘complex fluid’ effects are introduced through the ‘forcing’ term, eq.(49). These stability problems might be alleviated by providing ‘robust’ numerical schemes for advection and collision operators, like those discussed in section 3.2.2 and ref. [98].

The two-component version of the ‘HSD’ model (“He-Chen-Zhang extension”, see section 4.6) is close in spirit to the “front capturing” methods of the ‘NDIA’ (see Appendix

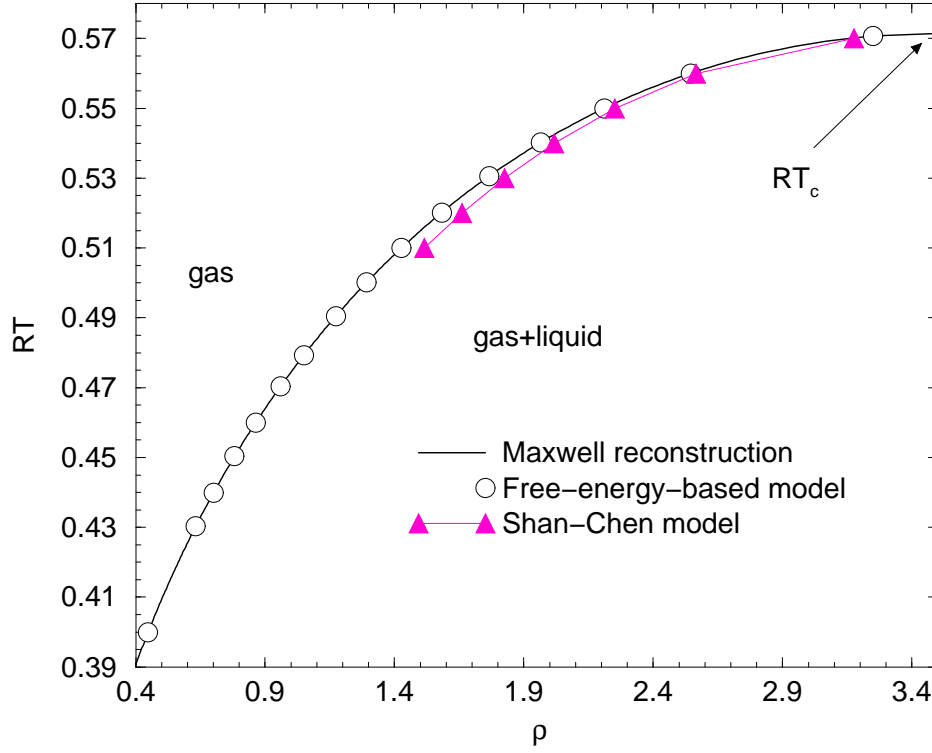


FIG. 5. Coexistence curve (gas branch), calculated by the “SC” and the “free-energy-based” models, [74]. Van der Waals fluid. T_c is a “critical temperature”.

C), where the “index” function ϕ eq.(56) effectively plays the role of the ‘volume-of-fluid’ or the ‘level set’ functions. In [40], this model has been used to simulate Rayleigh-Taylor instability. The results of the simulation are comparable with those obtained by the “continuum” CFD approaches, using the “VOF”, the “Level Set” and Tryggvason’s “front-tracking” methods. Fig.6 shows comparison of the HSD LBE model with the pseudocompressible NAR method, [75]. The later utilizes the level set function approach for “capturing” interface²⁴. While being able to describe basic numerical tests for multiphase flows with accuracy comparable to the LBE method (e.g., single-mode Rayleigh-Taylor instability, Fig.6), the NAR approach offers important flexibility currently not available in LBE. For example, implementation of variable fluid viscosity and heat transfer is straightforward. Perhaps more importantly, in NAR we have no constraints on the density ratio of the fluids across an interface, as applicable in all low-pressure liquid-gas systems. This is demonstrated by the dam-breaking problem (density ratio 1:1000) in Fig.7.

²⁴The “**Numerical Acoustic Relaxation**” (“**NAR**”) method is devised from the classical concept of “artificial compressibility” due to Chorin and combined with a ghost-fluid methodology and level-set algorithm for interface capturing and robust treatment of phase coupling. High accuracy and computational efficiency of the method are achieved by using a characteristics-based conservative finite-difference approach and introducing a generalized “time-stretching” scheme to solve the hyperbolic conservation laws. For details of implementation and validation see [75].

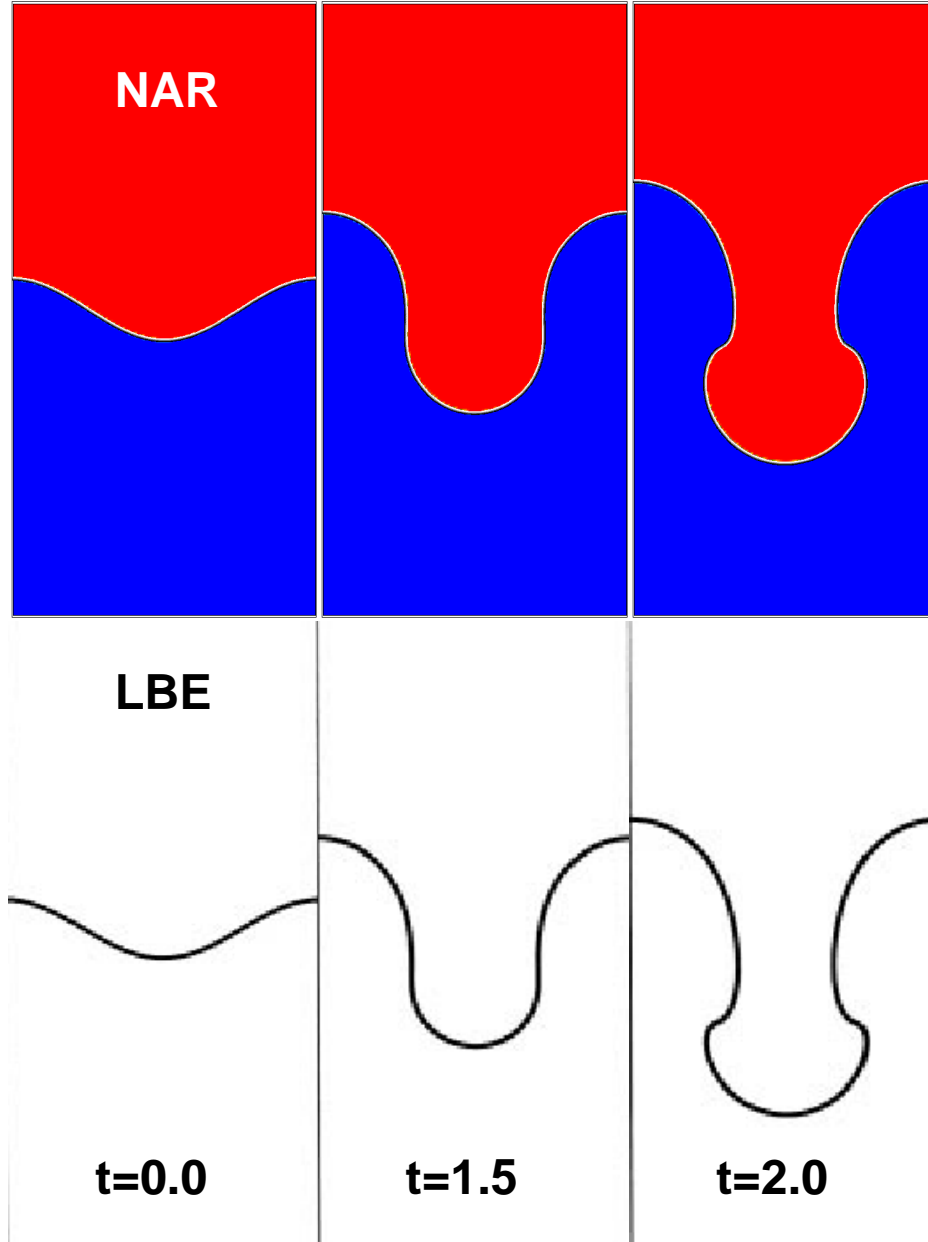


FIG. 6. Rayleigh-Taylor instability. Comparison of the “Level Set-NAR” [75] and the HSD-LBE [40] methods. Parameters of the test-case (“Level Set-NAR”/“HSD-LBE”): $At = 0.5$; $Re = 256$; single-mode initial perturbation with amplitude 10%; grid resolution - $(128 \times 256)_{\text{NAR}} / (256 \times 1056)_{\text{LBE}}$. The “upper” fluid has density $\rho = 3$; while the “lower” fluid has density $\rho = 1$.

4.7.4. Summary

On one hand, the LBE methods for fluid-fluid multiphase flows are able to reproduce several basic interfacial phenomena, such as spinoidal decomposition in binary fluids, oscillation of a capillary wave, Rayleigh-Taylor instability, etc., with the results comparable

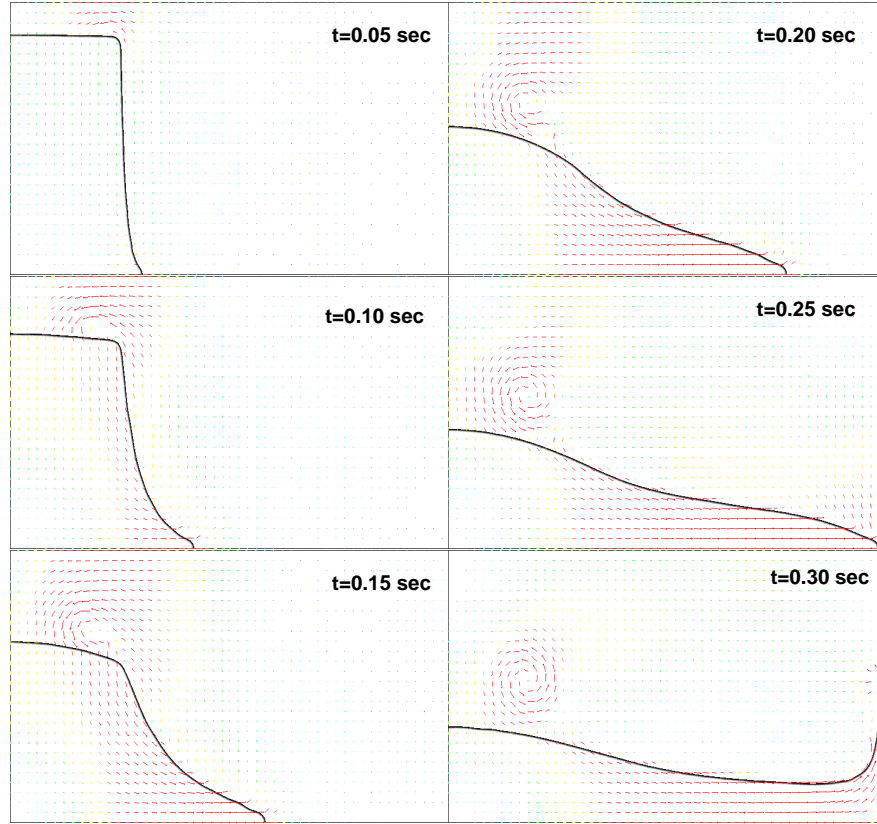


FIG. 7. Collapse of water column in a rectangular box using the “Level Set-NAR” approach. Density ratio is 1:1000. Dimensions of the water column and box are $L \times 2L$ and $4L \times 2.3L$, respectively. $L=14.6$ cm.

to those obtained by the methods of the “continuum” CFD. On the other hand, the currently existing multiphase LBE methods are not able to beneficially utilize the ‘kinetic theory origin’ of the method. That is, in order to simulate the interfacial phenomena, all currently existing LBE models practically employ the same techniques, as those used in the “continuum” CFD: *i.e.*, intermolecular interactions are implemented through the *phenomenological thermodynamical models* - equations of state; and the capillary effects are introduced by utilizing the “density gradient” approaches. Additionally, there are challenges to overcome in order to demonstrate the LBE scheme as a competitive methodology, comparing to the direct solution of the conservation equations of continuum mechanics. These include a consistent modeling of energy transport; elimination of excessive numerical discretization errors; and robustness and numerical stability under wide range of flow conditions and multiphase flow properties.

5. DERIVATION AND ANALYSIS OF THE CONTINUUM EQUIVALENT OF THE LB EQUATION

In the present section, we outline the major steps of the Chapman-Enskog expansion method, applied to the LBE BGK method, deriving the successive hierarchy of the LBGK equations, section 5.1. Then, the equations of hydrodynamics are derived and analyzed in sections 5.2-5.4.

5.1. Chapman-Enskog expansion method

The purpose of the Chapman-Enskog method is to solve Boltzmann equation by successive approximations. This shall yield solutions, that depend on time implicitly through the local density, velocity and temperature, $f(t) = f[\rho(t), \mathbf{u}(t), T(t)]$ - the ‘Chapman-Enskog *ansatz*’, [49]. In the present section, we outline the basic steps of the procedure, applied to the isothermal discrete Boltzmann equation (28).

First, we introduce a formal expansion of the discrete probability distribution function:

$$f_a = f_a^{(0)} + \varepsilon f_a^{(1)} + \varepsilon^2 f_a^{(2)} + \dots = \sum_{k=0}^{\infty} \varepsilon^k f_a^{(k)} \quad (60)$$

where ε is a lattice Knudsen number, eq.(26), which keeps track of the order of the terms in the series. The Chapman-Enskog expansion provides a consistent and practical definition of $f_a^{(k)}$ [49]. The functions $f_a^{(k)}$ are defined in such a way so that $f_a^{(k)}$ decreases as k increases. To satisfy eqs.(21), the first three moments of the zeroth approximation shall reproduce macroscopic density, velocity and kinetic energy, while corresponding moments of the higher-order terms are set to zero:

$$\begin{aligned} \sum_a f_a^{(0)} &= \rho; & \sum_a f_a^{(0)} e_{a_i} &= \rho u_i & \frac{1}{2} \sum_a f_a^{(0)} \cdot (e_{a_i} - u_i)^2 &= \rho \mathcal{E}; \\ \sum_a f_a^{(n)} &= 0; & \sum_a f_a^{(n)} e_{a_i} &= 0; & \sum_a f_a^{(n)} e_a^2 &= 0; \quad n > 0 \end{aligned} \quad (61)$$

LBE conservation laws. Substituting expansion eq.(60) into eq.(28)²⁵ and taking the first ‘discrete moment’ (\sum_a eq.(28)) result in the mass conservation equation

$$\begin{aligned} &\underline{\text{Mass conservation law:}} \\ &\partial_t \rho + \partial_j \rho u_j = 0 \end{aligned} \quad (63)$$

Taking the second ‘discrete moment’ (\sum_a eq.(28) $\times e_{a_i}$) yields the momentum conservation law:

$$\partial_t \rho u_i = -\partial_j \sum_{n=0}^{\infty} \varepsilon^n \sum_a e_{a_i} e_{a_j} f_a^{(n)} + \frac{a_j}{c_s^2} \left(\sum_a f_a^{\text{eq}} e_{a_i} e_{a_j} - \rho u_i u_j \right) \quad (64)$$

²⁵To avoid using expansions:

$$f_a(\mathbf{r} + \mathbf{e}_a \delta_t, t + \delta_t) = \sum_{k=0}^{\infty} \frac{\varepsilon^k}{k!} D_t^k f_a(\mathbf{r}, t); \quad D_t \equiv (\partial_t + \mathbf{e}_a \cdot \nabla) \quad (62)$$

traditionally employed to evaluate the ‘stream-and-collide’ advection operator, $\mathcal{A}(f) = f_a(\mathbf{r} + \mathbf{e}_a \delta_t, t + \delta_t) - f_a(\mathbf{r}, t)$, [41] [96], we assume that high-order finite-difference scheme is applied to the $\mathcal{A}(f_a) = \partial_t f_a + e_{a_j} \partial_j f_a$ (see section 3).

Introducing the n^{th} approximation of the pressure tensor as

$$\mathcal{P}_{i,j}^{(n)} \equiv \sum_a (e_{a_i} - u_i)(e_{a_j} - u_j) f_a^{(n)} \quad (65)$$

the momentum conservation equation (64) is re-arranged into the following form ²⁶:

$$\begin{aligned} & \text{\textit{Momentum conservation law:}} \\ \partial_t \rho u_i + \partial_j \rho u_i u_j = & -\partial_j \sum_{n=0}^{\infty} \varepsilon^n \mathcal{P}_{i,j}^{(n)} + \underbrace{\frac{a_j}{c_s^2} (\Pi_{i,j}^{\text{eq}} - \rho u_i u_j)}_{F_{i,j}} \end{aligned} \quad (66)$$

To derive the kinetic energy conservation equation, substitute expansion eq.(60) into eq.(28), then multiply it by $\frac{e_a^2}{2}$, and sum over all molecule directions. In addition, make use of the following equation:

$$\partial_t \sum_a f_a^{(0)} \frac{e_a^2}{2} = \partial_t \rho \mathcal{E} + u_i \partial_t \rho u_i - \frac{u^2}{2} \partial_t \rho \quad (67)$$

coming from the definition of the kinetic energy eq.(21) and constraints eq.(61). Also, introduce the n^{th} approximation of the heat flux as

$$Q_i^{(n)} \equiv \frac{1}{2} \sum_a (e_{a_i} - u_i)(e_{a_j} - u_j)^2 f_a^{(n)} \quad (68)$$

which allows to write the energy conservation equation as

$$\begin{aligned} & \text{\textit{Kinetic energy conservation law:}} \\ \partial_t \rho \mathcal{E} + \partial_j \rho \mathcal{E} u_j = & -\partial_j \sum_{n=0}^{\infty} \varepsilon^n Q_j^{(n)} - \partial_j u_i \cdot \sum_{n=0}^{\infty} \varepsilon^n \mathcal{P}_{i,j}^{(n)} \\ & + \underbrace{\frac{a_j}{c_s^2} \left[\sum_a f_a^{(\text{eq})} \left(\frac{(e_{a_j} - u_j)^2}{2} - e_{a_i} e_{a_j} u_i \right) + \rho u_j u^2 \right]}_{Q_j} \end{aligned} \quad (69)$$

LBE successive approximation. To obtain a consistent scheme of successive approximation, $f_a^{(n)}$ is defined in such a way that if all $f_a^{(k)}$, $\mathcal{P}_{i,j}^{(k)}$ and $Q_j^{(k)}$ are neglected for $k > n$, than we have the n^{th} approximation to the distribution function and to the hydrodynamic equations. To find such a definition, we decompose eq.(28) into successive equations for $f_a^{(n)}$ in the following manner.

1. Introduce expansion:

$$D f_a = D f_a^{(0)} + \varepsilon D f_a^{(1)} + \varepsilon^2 D f_a^{(2)} + \dots \quad (70)$$

Consistency of this expansion with eq.(60) follows from the linearity of the operator $D \equiv e_{a_j} \partial_j$.

²⁶Note, the following notation is in use: $\Pi_{i,j}^{\text{eq}} \equiv \sum_a f_a^{(\text{eq})} e_{a_i} e_{a_j}$.

2. Consider $\partial_t f_a$. Due to the ‘Chapman-Enskog *ansatz*’, f_a depends on time implicitly, only through the ρ , ρu_i and $\rho \mathcal{E}$. Thus,

$$\frac{\partial f_a}{\partial t} = \frac{\partial f_a}{\partial \rho} \frac{\partial \rho}{\partial t} + \frac{\partial f_a}{\partial \rho u_i} \frac{\partial \rho u_i}{\partial t} + \frac{\partial f_a}{\partial \rho \mathcal{E}} \frac{\partial \rho \mathcal{E}}{\partial t} \quad (71)$$

To expand eq.(71) into infinite series in powers of ε , expand $\frac{\partial f_a}{\partial \rho}$, $\frac{\partial f_a}{\partial \rho u_i}$ and $\frac{\partial f_a}{\partial \rho \mathcal{E}}$ as

$$\begin{aligned} \frac{\partial f_a}{\partial \rho} &= \frac{\partial f_a^{(0)}}{\partial \rho} + \varepsilon \frac{\partial f_a^{(1)}}{\partial \rho} + \varepsilon^2 \frac{\partial f_a^{(2)}}{\partial \rho} + \dots \\ \frac{\partial f_a}{\partial \rho u_i} &= \frac{\partial f_a^{(0)}}{\partial \rho u_i} + \varepsilon \frac{\partial f_a^{(1)}}{\partial \rho u_i} + \varepsilon^2 \frac{\partial f_a^{(2)}}{\partial \rho u_i} + \dots \\ \frac{\partial f_a}{\partial \rho \mathcal{E}} &= \frac{\partial f_a^{(0)}}{\partial \rho \mathcal{E}} + \varepsilon \frac{\partial f_a^{(1)}}{\partial \rho \mathcal{E}} + \varepsilon^2 \frac{\partial f_a^{(2)}}{\partial \rho \mathcal{E}} + \dots \end{aligned} \quad (72)$$

The expansions for time derivatives $\partial_t \rho$, $\partial_t \rho u_i$ and $\partial_t \rho \mathcal{E}$ must be defined to be consistent with the conservation laws eqs.(63), (66) and (69). Thus, the definition of $\frac{\partial_n}{\partial t}$ is taken from the n^{th} approximation to the conservation laws:

Mass conservation:

$$\begin{aligned} \partial_{t_0} \rho &\equiv -\partial_j \rho u_j \\ \partial_{t_n} \rho &\equiv 0; \quad (n > 0) \end{aligned} \quad (73)$$

Momentum conservation:

$$\begin{aligned} \partial_{t_0} \rho u_i &\equiv -\partial_j \rho u_i u_j - \partial_j \mathcal{P}_{i,j}^{(0)} + F_{i,j} \\ \partial_{t_n} \rho u_i &\equiv -\partial_j \mathcal{P}_{i,j}^{(n)}; \quad (n > 0) \end{aligned} \quad (74)$$

Energy conservation:

$$\begin{aligned} \partial_{t_0} \rho \mathcal{E} &\equiv -\partial_j \rho \mathcal{E} u_j - \partial_j \mathcal{Q}_j^{(0)} - \partial_j u_i \cdot \mathcal{P}_{i,j}^{(0)} + Q_j \\ \partial_{t_n} \rho \mathcal{E} &\equiv -\partial_j \mathcal{Q}_j^{(n)} - \partial_j u_i \cdot \mathcal{P}_{i,j}^{(n)}; \quad (n > 0) \end{aligned} \quad (75)$$

As a result, the following consistent expansion of ∂_t is obtained²⁷:

$$\partial_t = \partial_{t_0} + \varepsilon \partial_{t_1} + \varepsilon^2 \partial_{t_2} + \dots \quad (77)$$

3. With the defined expansions (60), (70) and (77), the LBE transport equation (28) can be written as²⁸:

$$\begin{aligned} &[(\partial_{t_0} + \varepsilon \partial_{t_1} + \varepsilon^2 \partial_{t_2} + \dots) + D] (f_a^{(0)} + \varepsilon f_a^{(1)} + \varepsilon^2 f_a^{(2)} + \dots) = \\ &= -\frac{1}{\varepsilon \tau} \left[(f_a^{(0)} + \varepsilon f_a^{(1)} + \varepsilon^2 f_a^{(2)} + \dots) - f_a^{\text{eq}} \right] + \frac{a_j}{c_s^2} (e_{a,j} - u_j) f_a^{\text{eq}} \end{aligned} \quad (78)$$

²⁷This formulation differs from [3] and [17], where the time derivative is expanded as

$$\partial_t = \varepsilon \partial_{t_1} + \varepsilon^2 \partial_{t_2} + \dots \quad (76)$$

²⁸Note, $(\dot{\cdot})$ is omitted.

4. To *uniquely* define $f_a^{(n)}$ we require that the coefficient of each power of ε vanish separately in eq.(78). Thus, the equations to be solved to yield all the $f_a^{(n)}$ are

Successive hierarchy of the LBGK equations:

$$\begin{array}{c|c}
 (\varepsilon^{-1}) : & f_a^{(0)} = f_a^{\text{eq}} \\
 & 0^{th}\text{-order: "Euler"} \\
 \hline
 (\varepsilon^0) : & \partial_{t_0} f_a^{(0)} + \mathbf{D} f_a^{(0)} = -\frac{f_a^{(1)}}{\tau} + \frac{a_j}{c_s^2} (e_{aj} - u_j) f_a^{(0)} \\
 & 1^{st}\text{-order: "Navier-Stokes"} \\
 \hline
 \dots & \dots \\
 & \text{High-order: "Burnett", "Super-Burnett", etc.} \\
 \dots & \dots \\
 (\varepsilon^k) : & \partial_{t_0} f_a^{(k)} + \partial_{t_1} f_a^{(k-1)} + \dots + \partial_{t_k} f_a^{(0)} + \mathbf{D} f_a^{(k)} = -\frac{f_a^{(k+1)}}{\tau} \\
 \dots & \dots
 \end{array} \quad (79)$$

In the Chapman-Enskog theory for the Boltzmann equation, in order to reproduce the Navier-Stokes equations, only the first two approximations $f_a^{(0)}$ and $f_a^{(1)}$ are required²⁹.

In the following section, we recover and analyze the equations of hydrodynamics corresponding to three most commonly used isothermal LBE models.

5.2. Hydrodynamic equations of the ‘ideal fluid’ LBGK model

Navier-Stokes equations. The governing equations of the compressible isothermal Newtonian fluid hydrodynamics are [63]

$$\begin{aligned}
 \partial_t \rho + \partial_j \rho u_j &= 0 \\
 \partial_t \rho u_i + \partial_j \rho u_i u_j &= -\partial_i P + \partial_j \mathcal{T}_{i,j} + \rho a_i
 \end{aligned} \quad (80)$$

where the viscous stress tensor has the following form [5] :

$$\mathcal{T}_{i,j} = \eta (\partial_j u_i + \partial_i u_j) + \underbrace{\left(\xi - \frac{2}{3} \eta \right)}_{\text{'Bulk' viscosity, } \lambda} \partial_k u_k \cdot \delta_{i,j} \quad (81)$$

and η and ξ are the ‘first’ and the ‘second’ fluid viscosities. Following Stokes, the ‘bulk’ and ‘second’ viscosities are $\lambda = -\frac{2}{3}\eta$ and $\xi = 0$, respectively, [5].

²⁹There exist fundamental difficulties when truncations of the Chapman-Enskog expansion are used beyond the Navier-Stokes order $f_a^{(1)}$, (‘Burnett-’ and ‘super-Burnett’ equations level). Notably, any truncation beyond $f_a^{(1)}$ is inconsistent with the Clausius-Duhem inequality, which is often taken as a representation of the second law of thermodynamics [89]. This fact was first noted for compressible gas dynamics by Bobylev [9] and later by Luk’shin [65]. Although the modifications of Navier-Stokes equations due to Burnett were expected to provide results superior to that of Navier-Stokes equations under high Kn numbers, present evidences indicate that this is not so; in fact, where the Navier-Stokes equations are themselves perhaps not completely adequate, the higher-order equations may even be inferior. Since the expansion eq.(60) is asymptotic; when the first two terms give a very good approximation, the third term may provide a further refinement. However, when the first two terms fail, inclusion of higher-order terms likely make matters worse; this is a known behavior in asymptotic series [33].

LBGK hydrodynamic equations^{30,31}. For the case of the “ideal-gas LBGK model”, the pressure tensor is given by

$$\hat{\mathcal{P}}_{i,j}^{(0)} = \hat{\rho} \hat{c}_s^2 \cdot \delta_{i,j} \quad (82)$$

Since the “zeroth-order solution of the LBGK equation”, eq.(79), is $\hat{f}_a^{(0)} = \hat{f}_a^{(\text{eq})}$, the momentum flux tensor is $\hat{\Pi}_{i,j}^{(0)} = \hat{\Pi}_{i,j}^{(\text{eq})}$. Thus, the momentum conservation equation (66), which is the “first-order solution of the LBGK equation”, eq.(79), is:

$$\partial_i \hat{\rho} \hat{u}_i + \partial_j \hat{\rho} \hat{u}_i \hat{u}_j = -\partial_i \hat{\rho} \hat{c}_s^2 - \partial_j \left(\underbrace{\varepsilon \hat{\mathcal{P}}_{i,j}^{(1)}}_{\substack{\text{Viscous stress} \\ \text{tensor, } -\hat{\mathcal{T}}_{i,j}^{\text{LBGK}}}} \right) + \hat{\rho} \hat{a}_i \quad (83)$$

Viscosity. The ‘first’ and the ‘second’ viscosities are defined as³²

$$\hat{\eta} = \hat{\tau} \varepsilon \hat{\rho} \hat{c}_s^2 = \underbrace{\frac{\tau \hat{c}_s^2 U_0}{L}}_{\frac{1}{\text{Re}}} \hat{\rho}; \quad \hat{\xi} = \frac{2}{3} \hat{\eta} \quad (84)$$

which renders the following definition of the dimensional kinematic viscosity:

$$\nu = \tau c_s^2 \quad (85)$$

An assumption of the constant temperature would require the following constraint be satisfied:

$$\begin{aligned} \partial_j \hat{\mathcal{Q}}_j^{(0)} &= -\varepsilon \partial_j \hat{\rho} \hat{u}_j - \partial_j \hat{u}_i \cdot \hat{\mathcal{P}}_{i,j}^{(0)} + \hat{Q}_j \\ \partial_j \hat{\mathcal{Q}}_j^{(1)} &= -\partial_j \hat{u}_i \cdot \hat{\mathcal{P}}_{i,j}^{(1)} \end{aligned} \quad (86)$$

For this LBGK model, the viscous stress term is (details of the derivation are given in Appendix D):

$$-\partial_j \left(\varepsilon \hat{\mathcal{P}}_{i,j}^{(1)} \right) = \partial_j \hat{\mathcal{T}}_{i,j}^{\text{LBGK}} = \partial_j \left[\hat{\mathcal{T}}_{i,j} \right] + \hat{\mathbf{A}}_{i,j}^{(\text{n.l.d.})} \quad (87)$$

where $\hat{\mathcal{T}}_{i,j}$ is the non-dimensional Navier-Stokes viscous stress tensor, defined by eq.(81); $\hat{\mathbf{A}}_{i,j}^{(\text{n.l.d.})}$ is a “non-linear³³ deviation” of this LBGK model from the classical Navier-Stokes

³⁰To avoid confusion, in the present section, we will use $(\hat{\cdot})$ to denote non-dimensional variables.

³¹In the following analysis, it is assumed that the lattice geometry is chosen in such a way so that $\Upsilon^{(4)} = \hat{c}_s^4$. (See appendix A for the lattice geometry).

³²Note, the $\hat{\xi}$ is not Stokesian, $\hat{\xi} \neq 0$. The value of the ‘second’ viscosity is not important as long as the velocity field is close to the ‘divergence-free’ condition of the incompressible fluid.

³³The term “non-linear” reflects the fact that the deviation is ‘cubic’ in velocity, $\sim u_j u_k$.

equations, given by

$$\begin{aligned} \hat{A}_{i,j}^{(n.l.d.)} = & \frac{1}{\text{Re } \hat{c}_s^2} \left[\partial_j (-2\hat{u}_i \hat{u}_j \hat{u}_k \partial_k \hat{\rho}) - \partial_j \hat{\rho} \cdot (\hat{u}_i \partial_k \hat{u}_k \hat{u}_j + \hat{u}_j \partial_k \hat{u}_k \hat{u}_i) - \right. \\ & \left. - \hat{\rho} \partial_j (\hat{u}_i \partial_j \hat{u}_k \hat{u}_j + \hat{u}_j \partial_i \hat{u}_k \hat{u}_i) \right] + \\ & + \frac{1}{\text{Re Fr } \hat{c}_s^4} \partial_j (\hat{\rho} \hat{u}_i \hat{u}_j \hat{u}_k \hat{i}_k) \end{aligned} \quad (88)$$

where $\text{Re} = \frac{\hat{\rho}}{\eta} = \frac{1}{\nu}$ and Fr are the Reynolds and Froude numbers, respectively.

Thus, the governing equations of this LBGK model are

$$\begin{aligned} \partial_i \hat{\rho} + \partial_j \hat{\rho} \hat{u}_j &= 0 \\ \partial_i \hat{\rho} \hat{u}_i + \partial_j \hat{\rho} \hat{u}_i \hat{u}_j &= -\partial_i \hat{P} + \partial_j \left[\frac{\hat{\rho}}{\text{Re}} (\partial_j \hat{u}_i + \partial_i \hat{u}_j) \right] + \frac{\hat{\rho}}{\text{Fr}} \hat{i}_i + \underbrace{\hat{A}_{i,j}^{(n.l.d.)}}_{\text{Non-linear deviations}} \end{aligned} \quad (89)$$

Linear Part: not quite Incompressible Navier-Stokes [see eq.(E.6)]

where \hat{i}_i is a unit vector specifying the orientation of the external body force.

The deviations of the continuum equivalent of this LBE model from the incompressible Navier-Stokes equations are detailed in Appendix E. From this, one can see the implication of \hat{c}_s , the dimensionless “pseudo-sound-speed”, introduced in eq.(28). In the linear term, it leads to the kinematic viscosity and Reynolds number that appears in front of the linear part. By appropriate choices of \hat{c}_s and $\hat{\tau}$, flow with any Reynolds number (any viscosity) can be modeled by eq.(14). On the other hand, in the non-linear (“cubic”) term, we are left with terms that contain, in addition to Re , \hat{c}_s^2 and \hat{c}_s^4 . Thus, we can make these terms as small as we wish by requiring that \hat{c}_s is chosen so that

$$(\text{Re } \hat{c}_s^2) \gg 1 \quad \text{and} \quad (\text{Re Fr } \hat{c}_s^4) \gg 1 \quad (90)$$

In fact, it turns out that these conditions are automatically satisfied as long as $\hat{c}_s \gg 1$, and the basic stability criterion for integration of the LBE, namely that $\frac{c_s \delta t}{\delta x} < 1$ are satisfied. To see this, take N as the number of lattice points in the cross-stream direction ($N \gg 1$), and suppose we chose $\frac{c_s \delta t}{\delta x} = \frac{1}{\sqrt{3}}$. We then have

$$\frac{1}{\text{Re } \hat{c}_s^2} = \frac{1}{\sqrt{3} N \hat{c}_s}$$

from which it is seen that the condition $\hat{c}_s \gg 1$ is moderate because $N \gg 1$. Also, you will note that for inertia flows, $\text{Re} \gg 1$, the condition on $\hat{c}_s \gg 1$ is moderate³⁴, but for viscous flows, $\text{Re} < 1$, we must obey a stronger condition on $\hat{c}_s \gg 1$, so that $\text{Re } \hat{c}_s^2 \gg 1$ and the “non-linear term” is smaller than the inertia “term”.

We have verified numerically that indeed, as long as these conditions and $\frac{\Delta \rho}{\rho} \ll 1$ are satisfied, exact solutions can be obtained arbitrarily close in Poiseuille and Couette flows,

³⁴The smallest term in the Navier-Stokes equations is of the order $\frac{1}{\text{Re}}$, thus, the requirement for \hat{c}_s is $\frac{1}{\text{Re}} \gg \frac{1}{\text{Re } \hat{c}_s^2}$

for any values of viscosity (or Reynolds number). Also note that, as appropriate for incompressible viscous flows, the pressure level is immaterial. If the pressure drop is specified, it implies a corresponding density drop, through eq.(82), and care must be exercised, because errors will be introduced unless $\frac{\Delta\rho}{\rho}$ remains much less than 1.

5.3. Hydrodynamic equations of the isothermal ‘HSD’ LBGK model for nonideal fluid

In the He-Shan-Doolen model, the pressure tensor and body force are given by

$$\begin{aligned} \mathcal{P}_{i,j}^{(0)} &= \rho c_s^2 \cdot \delta_{i,j} \\ F_{i,j} &= \rho a_j \delta_{i,j}; \quad a_j = \frac{-\partial_j P^* + \kappa \rho \partial_j \partial_k^2 \rho + \rho g_j}{\rho} \end{aligned} \quad (91)$$

where g_j is an acceleration due to the external body force; and the ‘non-ideal’ part of the equation of state P^* is given by, e.g., van der Waals eqs.(49) and (50). The distinguished feature of this model is that the non-ideal equation of state (pressure) is incorporated directly through the momentum source term. The momentum conservation equation, written in the “dimensional” form, is:

$$\begin{aligned} &\underbrace{\partial_t \rho u_i}_{\sim \mathbb{O}(1 + \delta\rho_t)} + \underbrace{\partial_j \rho u_i u_j}_{\sim \mathbb{O}(1 + \delta\rho_L)} = \underbrace{\rho g_i}_{\sim \mathbb{O}\left(\frac{1}{Fr}\right)} - \\ &\left[\underbrace{-\partial_i (\rho c_s^2 + P^*(\rho))}_{\substack{\text{Non-ideal gas} \\ \text{pressure}}} \right] \left[\underbrace{+\kappa \rho \partial_i \partial_j^2 \rho}_{\substack{\text{‘Capillary stress tensor’ } K_{i,j}}} \right] \left[\underbrace{-\partial_j \left(\rho_r U_0^2 \varepsilon \hat{\mathcal{P}}_{i,j}^{(1)} \right)}_{\substack{\text{Viscous stress} \\ \text{tensor, } -\mathcal{T}_{i,j}^{\text{LBGK}}}} \right] \\ &\left[\underbrace{\sim \mathbb{O}(\hat{e}_s^2 \delta\rho_L)} \right] \left[\underbrace{\sim \mathbb{O}\left(\frac{\delta\rho_L}{We}\right)} \right] \left[\underbrace{-\partial_j \mathcal{T}_{i,j}}_{\sim \mathbb{O}\left(\frac{1+\delta\rho_L}{Re}\right)} \right] \left[\underbrace{-A_{i,j}^{(1,d.)} - A_{i,j}^{(n,1,d.)}} \right] \end{aligned} \quad (92)$$

where the Weber number and density variations are defined as

$$\begin{aligned} We &\equiv \frac{\rho_r U_0^2 L}{\sigma} \\ \delta\rho_L &= \frac{\rho_l - \rho_v}{\rho_r} \quad \text{and} \\ \delta\rho_t &= \frac{\Delta_t \rho}{\rho_r} \end{aligned} \quad (93)$$

respectively; ρ_l and ρ_v are the saturation density of the liquid and vapor phase under chosen temperature T ; and $\Delta_t \rho$ is a scale of the density variation over characteristic time scale $t_0 \equiv \frac{L}{U_0}$. In the scaling analysis of eq.(92), the temporal and spatial derivatives of the density are estimated as

$$\begin{aligned} \partial_t \rho &\sim \frac{U_0 \Delta_t \rho}{L} \\ \partial_i \rho &\sim \frac{\rho_l - \rho_v}{L} \\ \partial_{ij} \rho &\sim \frac{\rho_l - \rho_v}{L^2} \quad \text{and} \\ \partial_{ijk} \rho &\sim \frac{\rho_l - \rho_v}{L^3} \end{aligned} \quad (94)$$

In addition, parameters κ , a and b are scaled as

$$\begin{aligned} \kappa &\sim \frac{L\sigma}{\rho_l^2} = \frac{L^2 U_0^2}{\rho_r We} \\ a &\sim \frac{c_s}{\rho_r} \quad \text{and} \\ b &\sim \frac{1}{\rho_r} \end{aligned} \quad (95)$$

respectively.

The ‘constant-temperature’ condition is defined by eq.(86). The viscous stress tensor $\mathcal{T}_{i,j}^{\text{LBGK}}$ is derived in appendix D. Choosing the lattice with $\Upsilon^{(4)} = \hat{c}_s^4$, the ‘first’ and the ‘second’ viscosities are defined by eq.(84).

The deviations of the continuum equivalent of this LBGK model from the incompressible Navier-Stokes equations are detailed in Appendix E.

5.4. Hydrodynamic equations of the isothermal ‘free-energy-based’ LBGK model for non-ideal fluid

The governing hydrodynamic equations of this LBGK model, written in the “dimensional form”, are^{35,36}:

$$\begin{aligned} \underbrace{\partial_t \rho}_{\sim \mathbb{O}(1 + \delta \rho_l)} + \underbrace{\partial_j \rho u_j}_{\sim \mathbb{O}(1 + \delta \rho_l)} &= 0 \\ \underbrace{\partial_t \rho u_i}_{\sim \mathbb{O}(1 + \delta \rho_l)} + \underbrace{\partial_j \rho u_i u_j}_{\sim \mathbb{O}(1 + \delta \rho_l)} &= - \underbrace{\partial_i P_0}_{\sim \mathbb{O}(\delta \rho_l \hat{c}_s^2)} \\ &+ \underbrace{\partial_j \left[\left(\kappa \rho \partial_k^2 \rho + \frac{\kappa}{2} (\partial_k \rho)^2 \right) \delta_{i,j} - \kappa \partial_i \rho \cdot \partial_j \rho \right]}_{\substack{\text{‘Capillary stress tensor’, } K_{i,j} \sim \mathbb{O}\left(\frac{\delta \rho_l (1 + \delta \rho_l)}{We}\right)}} - \underbrace{\partial_j \left(\rho_r U_0^2 \varepsilon \hat{\mathcal{P}}_{i,j}^{(1)} \right)}_{\substack{\text{Viscous stress} \\ \text{tensor, } -\mathcal{T}_{i,j}^{\text{LBGK}}}} \end{aligned} \quad (96)$$

Derivation of the viscous stress tensor $\mathcal{T}_{i,j}^{\text{LBGK}}$ is similar to that one for the “isothermal³⁷ ideal gas” model and given in appendix D:

$$\begin{aligned} \partial_j (\mathcal{T}_{i,j}^{\text{LBGK}}) &= \underbrace{\partial_j \mathcal{T}_{i,j}}_{\sim \mathbb{O}\left(\frac{1 + \delta \rho_l}{Re}\right)} + A_{i,j}^{(1.d.)} + A_{i,j}^{(n.l.d.)} \end{aligned} \quad (97)$$

³⁵The body force has not been incorporated in any existing variants of this model, $q_f = 0$.

³⁶In the present section, we use $(\hat{\cdot})$ to explicitly denote non-dimensional variables.

³⁷Even though the concept of temperature can be introduced in the pressure tensor, it causes violation of the energy conservation in the LBE discrete kinetic theory, eq.(69) [66]. The ‘constant-temperature’ condition eq.(86) cannot be satisfied. This is a generic problem for all “isothermal” LBGK models.

In the analysis of this model, we assumed that the lattice geometry is such, so $\Upsilon^{(4)} = \hat{c}_s^4$. With this, the following viscosities are obtained:

$$\eta = \underbrace{\tau c_s^2}_{\nu} \rho; \quad \xi = \eta \left(\underbrace{\frac{5}{3} + 2 \frac{a\rho}{c_s^2} - \frac{1}{1-b\rho} - \frac{\rho b}{(1-b\rho)^2}}_{\sim \mathbb{O}(1)} + \underbrace{\kappa \frac{\partial_l^2 \rho}{c_s^2}}_{\sim \mathbb{O}\left(\frac{\delta \rho_l}{c_s^2 We}\right)} \right) \quad (98)$$

Notably, the second viscosity is non-Stokesian³⁸. It is also dependent on the virial coefficients of the equation of state and second gradients of density.

The deviations of the continuum equivalent of this LBE model from the incompressible Navier-Stokes equations are detailed in Appendix E.

6. COMPUTATIONAL EFFICIENCY

In what follows, we will discuss ‘pros’ and ‘cons’ of the LBE method as a ‘Navier-Stokes solver’, in terms of its simplicity, efficiency and capability for an efficient parallelization.

Simplicity. Simplicity in implementation has been used as an argument in favor of the LBE method. The simplest “stream-and-collide” LBE algorithm with “bounceback” boundary condition formulation is indeed easier to program and handle than the “continuum” CFD algorithms for solving the Navier-Stokes equations, often involving the solution of the Poisson equation, sophisticated Riemann solvers to handle convective terms; the use of unstructured grids to accurately describe flow in complex geometry; etc. However, a fair comparison would instantly eliminate the illusion about the superior simplicity of the LBE method. In fact, direct counterparts of the LBE are the “compressible flow methods for incompressible flows”, such as, Chorin’s approach of “artificial compressibility” (AC). This method does not require Poisson equation solvers, and it is also very simple for implementation on a regular mesh, [75]. Recent development of the Chorin’s AC method is the “Numerical Acoustic Relaxation (NAR)” method. In [75], we utilized the NAR for different single- and multiphase flow problems, which include “Lid-Driven Cavity”, the “Doubly Periodical Shear Layer Flow”, “Rayleigh-Taylor Instability” and “Collapse of Water Column”, comparing it with the LBE and other methods of incompressible fluid dynamics. Based on our experience with both NAR and LBE, we have found no advantage of using discrete kinetic method over direct solution of the Navier-Stokes equations.

The elusive simplicity of the LBE approach further fades away when the LBE method is pushed to match requirements on accuracy and stability, typical for advanced CFD codes based on solving the Navier-Stokes equations. In fact, the LBE method is by far more

³⁸For this model, there are strong velocity divergence sources at the interface, making the second viscosity important.

complex when it has to operate on non-uniform, body-fitted or adaptive lattices, or to have high-order-accurate treatment of boundary conditions (see for review [16]).

Efficiency. Computational efficiency of the ‘isothermal’ LBE approach has been discussed in the literature. In particular, in [19], the three-dimensional LBE algorithm is reported to be 2.5 times faster than the pseudo-spectral method for incompressible flow, for low-Reynolds-number conditions.

Comparison of the LBE model with “continuum” CFD incompressible finite-volume (FVM) “projection” method (Patankar’s and Spalding’s SIMPLE algorithm [80]) using the multi-grid technique on block-structured grids was performed by Berndorf et al. [8]. A channel flow with obstacles has been chosen as the test-case. The results of the calculations indicate that when the number of obstacles is small, the FVM is more efficient than the LBE. In part, the performance of the LBE method is impeded by small time steps, needed to limit the unphysical compressibility effects via increase of the “pseudo-sound-speed” $c_s = \frac{\delta_\pi}{\sqrt{3\delta_t}}$. As geometrical complexity of the flow domain increases, the efficiency of the multigrid³⁹ Poisson solver decreases. There exists a break-even point between the multigrid FVM and the LBE, beyond which the LBE method is shown to be more efficient than the FVM in complex geometry.

As discussed in [75], there is no essential advantage of the LBGK schemes over the methods of ‘artificial compressibility’ (AC), for high- and moderate-Re-number flows. For massive calculations of flow in complex-geometry configurations, the AC methods are more efficient than the LBE approach, since a smaller number of governing equations is needed in the AC method⁴⁰ and smaller number of variables needed to be stored. For multi-component fluids, the LBE method involves PPDF for each component, further increasing the number of explicit equations solved and the memory storage requirements.

The LBE approach, however, might still be superior for *low-Re-number flows*, since there is practically no large-viscosity-related numerical stability limitations, which dwindle time step in explicit finite-difference schemes of the “continuum” CFD, $\delta_t \leq \frac{\delta_\pi^2}{\nu}$ (see discussion in section 5.2). Development of the “implicit LBGK schemes”, such as in [101], might give an additional advantage to the LBE simulation of the steady-state Stokesian flows and flows in porous media.

Parallelization. *Scalability* is a quantitative measure to evaluate the capability of an algorithm for parallelization. The scalability (\mathbb{S}) is defined as the product of the ratio of the computational times spent for the same computational task, $\frac{\mathbb{T}_1}{\mathbb{T}_2}$, and the correspondent ratio of the number of processors involved:

$$\mathbb{S} \equiv \frac{\mathbb{P}_2}{\mathbb{P}_1} \times \frac{\mathbb{T}_1}{\mathbb{T}_2}$$

³⁹Multigrid is currently the best available algorithm for solution of system of algebraic equations.

⁴⁰Comparing to the LBE, instead of solving a system of at least six explicit equations (D_2Q_6 scheme) for f_a ($a = 1, \dots, 6$), one has to deal with a system of 3 explicit macroscopic equations for $\mathbf{W} = (\rho; \rho u; \rho v)$. This ratio (3:6) gets worse in 3D: it becomes 4:14 even for D_3Q_{14} . For thermal LBGK models, the minimum number of discrete velocities is 16 in 2D and 40 in 3D [17], thus, the ratio is 4:16 and 5:40, respectively (see also [72]).

where \mathbb{P} is the number of processors involved in the calculation. In the “ultimate parallelization” case, $\mathbb{S} = 1$. Parallelization of the LBE algorithm can be achieved by dividing the computational domain into \mathbb{P} subdomains, corresponding to \mathbb{P} processors available; solving for each subdomain on separate processor; and communicating data between processors using MPI [74]. This parallelization strategy is employed in many modern CFD codes [73]. We analyzed the scalability of the LBE method [74] and the “continuum” CFD finite-difference code for compressible fluid dynamics [73], [75], and found the scalability of both methods in the range 0.7 - 0.95. The LBE method involves a more complex stencil, and, thus, the network for inter-processor communication is more sophisticated. In two dimensions, each processor, instead of four neighbors of the “continuum” CFD finite-difference code ⁴¹, the D_2Q_9 LBE code requires eight neighbors⁴². More sophisticated processor-network is required in three dimensions, fig. 1b. Closely related to this is the amount of information to be ‘exchanged’ at the end of each time step. In the case of the LBE’s “stream-and-collide” D_2Q_9 scheme, symbolically, 3×8 float variables are being sent/received, corresponding to three “streamed” PPDFs, f_a , and eight neighbor-processors. For the finite-difference code, 3×12 variables must be sent/received, corresponding to three conserved variables ($\rho; u; v$) and [4 ‘neighbor-processors’ \times 3 layers of the finite-difference stencil ⁴³]. Based on the above consideration, one can see that the LBE approach is not an advantageous scheme.

In summary, the LBE method is a “pseudocompressible” solver of incompressible flows. It shares the advantages, disadvantages and limitations of this class of the computational fluid dynamics methods. This includes the simplicity and explicitness of the algorithm, which requires no solution of the Poisson equation; the restrictive simulation time step in order to maintain the low-Mach-number limit (incompressible flow); and the artificial compressibility effects, $\nabla \cdot \mathbf{u} = u_j \partial_j \ln \rho - \partial_t \ln \rho \neq 0$, originating from both the linearized “pseudo-equation of state” $P_{t/d} = c_s^2 \rho$ and the discretization errors. Similarly to the “pseudocompressible” methods of the continuum-based CFD, the LBE approach is efficient in parallelization and *suitable for massive computation of incompressible flows in complex geometry configurations*, such as flow in porous media, particulate and suspension multiphase flows.

7. CONCLUDING REMARKS

- The Lattice Boltzmann Equation (LBE) method is an alternative numerical scheme for description of incompressible hydrodynamics. The LBE method has potential to serve as an efficient solver for incompressible low-Re-number flows in complex geometries, including porous media, particulate/suspension multiphase flows.

- Computationally, the LBE method belongs to a class of the pseudocompressible solvers of the Navier-Stokes equations for incompressible flow. As such, the LBE method possesses the advantages (simplicity of algorithm, no Poisson equation solver) and limitations (re-

⁴¹We utilize the high-order-accurate (WENO₅, [53]) conservative finite-difference characteristics-based approach ([73]; [28]; [75]).

⁴²See the “stencil” of the D_2Q_9 in fig. 1a.

⁴³The ‘size’ of the stencil for WENO₅ scheme is 3 [53].

strictive time step, artificial compressibility) characteristic of pseudocompressible methods.

- Beyond the incompressible homogeneous fluid, the LBE method permits implementation of phenomenological terms and rules to mimic complex-fluid behaviors in a capacity similar to that of the continuum-based models of hydrodynamics. In this respect, the LBE models so far failed to provide a consistent framework for intermolecular interactions by making use of the discrete kinetic origin of the LBE method. Application of the LBE methods to multiphase situations is additionally limited by the admissible range of fluid properties (density ratio, surface tension and kinematic viscosity); time and length scales; and the inability to represent energy transport.

Acknowledgement. This work was supported in part by the National Aeronautics and Space Administration under grant No. NAG3-2119, Lawrence Livermore National Laboratory Contract B502686, and by the U.S. Nuclear Regulatory Commission under Cooperative Agreement No. NRC-04-98-051. The interest and therefore collaboration of D. Joseph was limited to the part of this paper dealing with homogeneous (single-phase) flows. This paper grew out of an informal memo by D. Joseph “General Remarks and Questions about the Lattice Boltzmann Method”, in which various flaws in the presentation of the LBE method were highlighted. The work of D. Joseph was supported by the NSF, Fluid, Particulate and Hydraulic Systems and by the Engineering Research Program of the Office of Basic Energy Sciences at the DOE.

REFERENCES

1. Aidun, C.K., and Lu, Y., Lattice-Boltzmann Simulation of Solid Particles Suspended in Fluid, *Journal Statistical Physics*, **81**, 49-61, 1995.
2. Aidun, C.K., Lu, Y., and Ding, E., Direct Analysis of Particulate Suspensions With Inertia Using the Discrete Boltzmann Equation, *J. Fluid mech.*, **373**, 287-311, 1998.
3. Alexander, F.J., Chen, S., and Sterling, J.D., Lattice Boltzmann Thermohydrodynamics, *Physical Review E*, **47** (4), R2249-R2252.
4. Andersen, D.M., McFadden, G.B., and Wheeler, A.A., Diffuse-Interface in Fluid Mechanics, *Annual Review of Fluid Mechanics*, **30**, 139-165, 1998.
5. Aris, R., *Vectors, Tensors, and the Basic Equations of Fluid Mechanics*, Prentice-Hall, Inc., Englewood Cliffs, N.J., 1962.
6. Batchelor, G.K., *An Introduction to Fluid Dynamics*, Cambridge: Cambridge University Press, 1967.
7. Bhatnagar, P.L., Gross, E.P., and Krook, M., Model for Collision Processes in Gases, *Phys. Rev.*, **94**, 511, 1954.
8. Bernsdorf, J., Durst, F., and Schäfer, A., Comparison of Cellular Automata and Finite Volume Techniques for Simulation of Incompressible Flows in Complex Geometries, *Int. J. for Numer. Meth. Fluids*, **29**, 251-264, 1999.
9. Bobylev, A.V., The Chapman-Enskog and Grad methods for Solving the Boltzmann Equation, *Sov. Phys. Dokl.*, **27**, 1982.
10. Boghosian, B.M., and Coveney, P.V., Inverse Chapman-Enskog Derivation of the Thermohydrodynamic Lattice-BGK Model for the Ideal Gas, *International Journal of Modern Physics C*, **9** (8), 1231-1245, 1998.
11. Bogoliubov, N.N., Problems of a Dynamical Theory in Statistical Physics, Moscow, 1946, (English transl. in “Studies in Statistical Mechanics”, J. De Boer and G.E. Uhlenbeck, eds., Vol. I, North-Holland Publ., Amsterdam, 1962).
12. Boltzmann, L., Weitere Studien über das Wärmegleichgewicht unter Gasmoleculen, *Wien Ber.*, **66**, 275, 1872. Translation in English can be found in: Brush, S.G., *Selected Readings in Physics, Kinetic Theory, Volume 2. Irreversible Processes*. Boltzmann, L., “Further Studies on the Thermal Equilibrium of Gas Molecules”, pp.88-175, 1966 Pergamon Press Ltd.
13. Cahn, J. W., and Hilliard, J. E., Free Energy of a Nonuniform System. 1. Interfacial Free Energy. *J. Chem. Phys.*, **28**(2), 258-267 (1958).

14. Cercignani, C., *Mathematical Methods in Kinetic Theory*, Plenum Press, New York, 1969.
15. Chapmann, S., and Cowling, T.G., *The Mathematical Theory of Non-Uniform Gases*, Cambridge University Press, 1970.
16. Chen, S., and Doolen, G. D., Lattice Boltzmann Method for Fluid Flows, *Annu. Rev. Fluid Mech.*, **30** (4), 329-364.
17. Chen, Y., Ohashi, H., and Akiyama, M., Thermal Lattice Bhatnagar-Gross-Krook Model Without Nonlinear Deviations in Macrodynamic Equations, *Physical Review E*, **50** (4), 2776-2783.
18. Chen, Y., and Ohashi, H., Lattice-BGK Methods for Simulating Incompressible Fluid Flows, *International Journal of Modern Physics C*, **8** (4), 793-803.
19. Chen, S., Wang, Z., Shan, X., and Doolen, G.D., Lattice Boltzmann Computational Fluid Dynamics in Three Dimensions, *Journal of Statistical Physics*, **68** (3/4), 379-400.
20. Chorin, A.J., A Numerical Method for Solving Incompressible Viscous Flow Problems, *Journal of Computational Physics*, **2**, 12, 1967. Recent edition: **135**, 118-125, 1997.
21. Cohen, E.G.D., Bogolubov and Kinetic Theory: The Bogolubov Equations, *Mathematical Models & Methods in Applied Sciences*, **7**(7) (1997), 909-933.
22. Dell'Isola, F., Gouin, H., and Seppecher, P., Radius and Surface Tension of Microscopic Bubbles by Second Gradient Theory, *C. R. Acad. Sci. Paris*, **320**, 211-216.
23. Ding, E. and Aidun, C.K., The dynamics and scaling law for particles suspended in shear flow with inertia, *J. Fluid Mech.*, **423**, 317-344, 2000.
24. Drew, D.A., Passman, S.L., *Theory of Multicomponent Fluids*, *Applied Mathematical Sciences* 135, Springer, 1999.
25. Eggels, J.G.M., Direct and Large-Eddy Simulation of Turbulent Fluid Flow using the Lattice-Boltzmann Scheme, *Int. J. Heat and Fluid Flow*, **17** (1996), 307-323.
26. Eggels, J.G.M., and Somers, J.A., Numerical Simulation of Free Convective Flow using the Lattice-Boltzmann Scheme, *Int. J. Heat and Fluid Flow*, **16** (1995), 357-364.
27. Enskog, D., *Kungl. Svenska Vetenskaps Akademiens Handl.*, **63**(4), 1921.
28. Fedkiw, R., Merriman, B., Donat, R., and Osher, S., The Penultimate Scheme for Systems of Conservation Laws: Finite Difference ENO with Marquina's Flux Splitting, *Progress in Numerical Solutions of Partial Differential Equations*, Arcachon, France, edited by M. Hafez, July 1998.
29. Felderhof, B.U., Dynamics of the diffuse gas-liquid interface near the critical point, *Physica*, **48** (1970), 541-560.
30. Feng, J., Hu, H.H., and Joseph, D.D., Direct Simulation of Initial Value Problems for the Motion of Solid Bodies in a Newtonian Fluid. Part 2. Couette and Poiseuille Flows, *J. Fluid mech.*, **277**, 271-301, 1994.
31. Frisch, U., Hasslacher, B., and Pomeau, Y., Lattice gas Cellular Automata for the Navier-Stokes equations, *Phys. Rev. Lett.*, **56** (1986), 1505.
32. Gibbs, J.W., On the equilibrium of heterogeneous substances, *Trans. Conn. Acad.*, 3:108-248, 3:343-524, 1878. Reprinted in *The Scientific Papers of J. Willard Gibbs*, pp.55-371. London: Longmans, Green, and Co, 1906.
33. Goldstein, S., Burgers, J.M., *Lectures on Fluid Mechanics*, Interscience Publishers, Ltd., London, 1957.
34. Gonnella, G., Orlandini, E., and Yeomans, J.M., Lattice-Boltzmann Simulation of Complex Fluids, *International Journal of Modern Physics*, **8**(4), 783-792.
35. Grad, H., On the Kinetic Theory of Rarified Gases, *Communications on Pure and Applied Mathematics*, **2**(4), pp.331-407, 1949.
36. Guangwu, Y., Yaosong, C., and Shouxin, H., Simple Lattice Boltzmann Model for Simulating Flows with Shock Wave, *Physical Review E*, January 1999, **59** (1), 454-459.
37. Gurtin, M.E., Polignone, D., and Vinals, J., Two-Phase Binary Fluids and Immiscible Fluids Described by an Order Parameter, *Mathematical Models and Methods in Applied Sciences*, **6**, 815 (1996).
38. Gustensen, A.K., Rothman, D.H., Zaleski, S., and Zanetti, G., Lattice Boltzmann Model of Immiscible Fluids, *Phys. Rev. A*, **43**, 4320-4327 (1991).
39. Harris, S., *An Introduction to the Theory of the Boltzmann Equation*, Holt, Rinehart and Winston, New York, 1971.
40. He, X., Chen, S., and Zhang, R., A Lattice Boltzmann Scheme for Incompressible Multiphase Flow and Its Application in Simulation of Rayleigh-Taylor Instability, *Journal of Computational Physics*, **152**, 642-663 (1999).

41. He, X., and Luo, L. -S., Lattice Boltzmann Model for the Incompressible Navier-Stokes Equation, *Journal of Statistical Physics*, **88** (3/4), 1997, 927-944.
42. He, X., and Luo, L. -S., *A priori* Derivation of the Lattice Boltzmann Equation, *Physical Review E*, June 1997, **55** (6), 6811-6817.
43. He, X., and Luo, L. -S., Theory of the Lattice Boltzmann: From the Boltzmann Equation to the Lattice Boltzmann Equation, *Physical Review E*, December 1997, **56** (6), 6811-6817.
44. He, X., Shan, X., and Doolen, G., Discrete Boltzmann equation model for nonideal gases, *Physical Review Letters*, January 1998, **57** (1), R13-R16.
45. He, X., *Private communication*.
46. Hirt, C.W., Nichols, B.D., Volume of Fluid (VOF) methods for the dynamics of free boundaries, *Journal of Computational Physics*, **39**, 201-225.
47. Hohenberg, B.I., and Halperin, P.C., Theory of Dynamic Critical Phenomena, *Reviews of Modern Physics*, **49**(3), 435-479 (1977).
48. Holdych, D.J., Rovas, D., Geogiadis, J.G., and Buckius, R.O., An improved Hydrodynamic Formulation for Multiphase Flow Lattice Boltzmann Models, *International Journal of Modern Physics C*, **9**(8), 1393, (1998).
49. Huang, K., Statistical Mechanics, *John Wiley & Sons, Inc.*, 1963.
50. Huang, J., Xu, F., Vallieres, H., Feng, D.H., Qian, Y.-H., Fryxell, B., and Strayer, M.R., A Thermal LBGK Model for Large Density and Temperature Differences, *International Journal of Modern Physics C*, **8** (4), 827-841, 1997.
51. Ishii, M., Thermo-Fluid Dynamic Theory of Two-Phase Flow, *Direction des Etudes et Recherches d'Electricité de France*, 1975.
52. Jacqmin, D., An Energy Approach to the Continuum Surface Tension Method, *AIAA 96-0858*, In *Proceedings of the 34th Aerospace Sciences Meeting and Exhibit*. Reno: American Institute of Aeronautics and Astronautics.
53. Jiang, G.S., and Shu, C.-W., Efficient Implementation of Weighted ENO Schemes, *Journal of Computational Physics*, **126**, 202-228, 1996.
54. Kirkwood, J.G., The Statistical Mechanical Theory of Transport Processes 2. Transport in Gases, *J. of Chemical Physics*, **15**(1), pp.72-76, 1947.
55. Koga, T., Introduction to Kinetic Theory Stochastic Processes in Gaseous Systems, *Pergamon Press*, 1970.
56. Korteweg, D.J., Sur la forme que prennent les équations du mouvements des fluides si l'on tient compte des forces capillaires causées par des variations de densité considérables mais continues et sur la théorie de la capillarité dans l'hypothèse d'une variation continue de la densité, *Arch. Néerl. Sci. Exactes Nat. Ser.*, II 6, 1-24, 1901.
57. Klimontovich, Yu.L., Turbulent Motion and Chaos Structure: A New Approach to Statistical Theory of Open Systems, *Nauka*, Moscow, (in Russian) 1990.
58. Ladd, A.J.C., Numerical Simulation of Particulate Suspensions via a Discretized Boltzmann Equation, Part 1. Theoretical Foundation, *J. Fluid Mech.*, **271**, 285-310, 1994.
59. Ladd, A.J.C., Numerical Simulation of Particulate Suspensions via a Discretized Boltzmann Equation, Part 2. Numerical Results, *J. Fluid Mech.*, **271**, 285-310, 1994.
60. Lallemand, P., and Luo, L.-S., Theory of the Lattice Boltzmann Method: Dispersion, Dissipation, Isotropy, Galilean Invariance, and Stability, *Physical Review E*, June 2000, **61** (6), 6546-6562.
61. Lamb, H., "*Hydrodynamics*", Cambridge: Cambridge University Press, 1932.
62. Lamura, A., Gonnella, G., and Yeomans, J.M., A Lattice Boltzmann Model of Ternary Fluid Mixtures, *Europhysics Letters*, 1 February 1999, **99** (3), 314-320.
63. Landau, L. D., and Lifschitz, E. M., *Theoretical Physics*, v.VI, "*Hydrodynamics*", Chapter II.15, In Russian, Nauka, Fourth Edition, 1988, Moscow.
64. Liboff, R.L., Introduction to the Theory of Kinetic Equations, *John Wiley & Sons, Inc.*, 1969.
65. Luk'shin, A.V., Hydrodynamical Limit for the Boltzmann Equation and its Different Analogs, in *Numerical Methods in Mathematical Physics*, Moscow State University, Moscow (1986), 61-91.
66. Luo, L.-S., Unified Theory of Lattice Boltzmann Models for Nonideal Gases, *Physical Review Letters*, 24 August 1998, **81** (8), 1618-1621.
67. Martys, N.S., and Chen, H., Simulation of Multicomponent Fluids in Complex Three-Dimensional Geometries by the Lattice Boltzmann Method, *Phys. Rev. E*, **53**, (1996), 743-750.

68. Maxwell, J.C., Capillary Action. In *Encyclopaedia Britannica*, (9th edition). Reprinted in *The Scientific Papers of James Clerk Maxwell*, **2**, pp.541-591. New York: Dover, 1952.
69. McNamara, G.R. and Zanetti, G., Use of the Boltzmann Equation to Simulate Lattice-Gas Automata, *Phys. Rev. Lett.*, **61**, Number 20, (1988), 2332.
70. McNamara, G.R. and Alder, B., Analysis of the Lattice Boltzmann Treatment of Hydrodynamics, *Physica A*, **194**, (1993), 218-228.
71. McNamara, G.R., Garcia, A.L., and Alder, B.J., Stabilization of Thermal Lattice Boltzmann Models, *Journal of Statistical Physics*, **81**, Number 1/2, (1995), 395-408.
72. McNamara, G.R., Garcia, A.L., and Alder, B.J., A Hydrodynamically Correct Thermal Lattice Boltzmann Model, *Journal of Statistical Physics*, **87**, Number 5/6, (1997), 395-408.
73. Nourgaliev, R.R., Dinh, T.A., Dalal, D.C., Dinh, T.N., and Theofanous, T.G., MuSiC: Multiscale Simulation Code. "Modeling of Complex Fluid-Fluid and Fluid-Solid Interactions using the Level Set and 'Ghost Fluid' Methodology. Single- and Multiphase Compressible Flows", UCSB-CRSS Research Report, November 20, 2000, 209p.
74. Nourgaliev, R.R., Dinh, T.N., and Sehgal, B.R., On Lattice Boltzmann Modeling of Phase Transitions in an Isothermal Non-Ideal Fluid, *Nuclear Engineering and Design*, **211**, (2002), 153-171.
75. Nourgaliev, R.R., Dinh, T.N., and Theofanous, T.G., The 'Numerical Acoustic Relaxation (NAR)' Method for Time-Dependent Incompressible Single- and Multiphase Flows, CD-ROM Proceedings of *The Fourth International Conference on Multiphase Flows*, May-June 2001, New Orleans, USA.
76. Oran, E. S., and Boris, J. P., Numerical Simulation of Reactive Flow, *Elsevier Science Publishing Co., Inc.*, New York-Amsterdam-London, 1987.
77. Qian, Y.H., D'Humières, D., and Lallemand, P., Lattice BGK Models for Navier-Stokes Equation, *Europhysics Letters*, **17** (6), 479-484.
78. Qian, Y. H., and Orszag, S.A., Lattice BGK Models for the Navier-Stokes Equation: Nonlinear Deviation in Compressible Regimes, *Europhys. Lett.*, **21**(3), 255-259, 1993.
79. Qian, Y. H., and Zhou, Y., Complete Galilean-Invariant Lattice BGK Models for the Navier-Stokes Equation, *NASA/CR-1998-208701*, ICASE Report No.98-38, August 1998.
80. Patankar, S.V., and Spalding, D.B., A Calculation Procedure for Heat, Mass and Momentum Transfer in Three-Dimensional Parabolic Flows, *Int. J. Heat Mass Transf.*, **15**, 1787-1806, 1972.
81. Poisson, S.D., *Nouvelle Théorie de l'action capillaire*, Paris: Bachelier, 1831.
82. Lord Rayleigh, On the theory of surface forces. - II. Compressible fluids. *Phil. Mag.*, **33**, pp.209-220, 1892.
83. Rider, W. J. , Approximate Projections Methods for Incompressible Flow: Implementation, Variants and Robustness, *Technical Report LA-UR-2000*, Los Alamos National Laboratory, 1994. Available on World Wide Web at <http://www.c3.lanl.gov/cic3/publications/main.html>.
84. Rothman, D.H., and Zaleski, S., *Lattice-Gas Cellular Automata: Simple models of complex hydrodynamics*, Cambridge University Press, 1997.
85. Schulkes, R.M.S.M., The Evolution and Bifurcation of a Pendant Drop, *J. Fluid Mech.*, **278**, 83, 1994.
86. Sehgal, B.R., Nourgaliev, R.R., and Dinh, T.N., Numerical Simulation of Droplet Deformation and Break-Up by Lattice-Boltzmann Method, *Progress in Nuclear Energy*, **34**(4), pp.471-488, 1999.
87. Seppecher, P., Moving Contact Lines in the Cahn-Hilliard Theory, *Int. J. Engng. Sci.*, **34** (9), 977-992, 1996.
88. Sethian, J.A., Level Set Methods and Fast Marching Methods, *Cambridge University Press*, 1999.
89. Slemrod, M., Constitutive Relations for Monoatomic Gases Based on a Generalized Rational Approximation to the Sum of the Chapman-Enskog Expansion, *Arch. Rational Mech. Anal.*, **150**, 1-22, 1999.
90. Shan, X. and Chen, H., Lattice Boltzmann Model for Simulating Flows with Multiple Phases and Components, *Physical Review E*, March 1993, **47** (3), 1815-1819.
91. Shan, X. and Chen, H., Simulation of Nonideal Gases and Liquid-Gas Phase Transitions by the Lattice Boltzmann Equation, *Physical Review E*, April 1994, **49** (4), 2941-2948.
92. Shan, X. and Doolen, G., Multicomponent Lattice-Boltzmann Model with Interparticle Interactions, *Journal of Statistical Physics*, **81** (1/2), 379-393.
93. Shan, X. and Doolen, G., Diffusion in a Multicomponent Lattice Boltzmann Equation Model, *Physical Review E*, October 1996, **54** (4), 3614-3620.
94. Sterling, J.D., and Chen, S., Stability Analysis of Lattice Boltzmann Methods, *Journal of Computational Physics*, **123**, 196-206, 1996.

95. Sun, C., Adaptive Lattice Boltzmann Model for Compressible Flows: Viscous and Conductive Properties, *Physical Review E*, March 2000, **61** (3), 2645-2653.
96. Swift, M. R., Osborn, W. R. and Yeomans, J. M., Lattice Boltzmann Simulations of Nonideal Fluid, *Physical Review E*, November 1996, **54** (5), 5041-5052.
97. Swift, M. R., Orlandini, E., Osborn, W. R. and Yeomans, J. M., Lattice Boltzmann Simulations of Liquid-Gas and Binary Fluid Systems, *Physical Review Letters*, 31 July 1995, **75** (5), 830-833.
98. Teng, S. L., Chen, Y., and Ohashi, H., Lattice Boltzmann Simulation of Multiphase Fluid Flows through the Total Variation Diminishing with Artificial Compression Scheme, *Int. J. of Heat and Fluid Flow*, **21**, 112-121, 2000.
99. Unverdi, S.O., Tryggvason, G., A Front-Tracking Method for Viscous, Incompressible, Multi-Fluid Flows, *Journal of Computational Physics*, **100**, 25-37, 1992.
100. van der Waals, Verhandel. Konink. Akad. Weten. Amsterdam (Sect. 1), vol. 1, No. 8 (Dutch). Transl. J.S. Rowlinson, 1979, Translation of J.D. van der Waals' "The thermodynamic theory of capillarity under the hypothesis of a continuous density variation", *J. Stat. Phys.*, **20**, 197-244.
101. Verberg, R., and Ladd, A.J.C., Simulation of Low-Reynolds-Number Flow via a Time-Independent Lattice-Boltzmann Method, *Physical Review E*, **60** (3), 3366-3373.
102. Wagner, A.J., and Yeomans, J.M., Effect of Shear on Droplets in a Binary Mixture, *International Journal of Modern Physics C*, **8** (4), 773-782.
103. Wolfram, S., Cellular Automata Fluids 1: Basic Theory, *Journal of Statistical Physics*, **45** (3/4), 471-526.
104. Yang, Z.L., Dinh, T.N., Nourgaliev, R.R., and Sehgal, B.R., Numerical Investigation of Bubble Growth and Detachment by the Lattice-Boltzmann Method, *International Journal of Heat and Transfer*, **44**, pp.195-206, 2001.
105. Zhang, D.F., Stone, H.A., Drop formation in viscous flows at a vertical capillary tube, *Phys. Fluids*, **9**, 2234, 1997.

APPENDIX A

Lattice geometry and symmetry

Consider the lattice composed of r sublattices in \mathcal{D} dimensions. Each sublattice has weight w_a , which is chosen to satisfy certain symmetry requirements. In total, the lattice has $a = 0, \dots, b$ links, \mathbf{e}_a .

The most important properties of the lattice are related to the symmetries of the tensors:

$$\mathbb{L}_{i_1 i_2 \dots i_n}^n = \sum_a w_a (|\mathbf{e}_a|^2) (\mathbf{e}_a)_{i_1} \dots (\mathbf{e}_a)_{i_n} \quad (\text{A.1})$$

which are determined from the choice of the basic lattice directions \mathbf{e}_a .

The basic condition for standard hydrodynamic behaviour is that tensors $\mathbb{L}^{(n)}$ for $n \leq 4$ should be isotropic [103]. Isotropic tensors $\mathbb{L}^{(n)}$, obtained with sets of b vectors \mathbf{e}_a composing r sublattices in \mathcal{D} space dimensions, must take the form

$$\begin{cases} \mathbb{L}^{(2n+1)} &= 0 \\ \mathbb{L}^{(2n)} &= \Upsilon^{(2n)} \Delta^{(2n)} \end{cases} \quad (\text{A.2})$$

where

$$\begin{cases} \Delta_{i,j}^{(2)} &= \delta_{ij} \\ \Delta_{i,j,k,l}^{(4)} &= \delta_{ij} \delta_{kl} + \delta_{ik} \delta_{jl} + \delta_{il} \delta_{jk} \\ \Delta_{i_1 i_2 \dots i_{2n}}^{(2n)} &= \sum_{j=2}^{2n} \delta_{i_1 i_j} \Delta_{i_2 \dots i_{j-1} i_{j+1} \dots i_{2n}}^{(2n-2)} \end{cases} \quad (\text{A.3})$$

Coefficients $\Upsilon^{(2n)}$ in eq.(A.2) are dependent on the specific lattice geometry, and are given in Table 1 for the most commonly used lattices.

APPENDIX B

Equilibrium distribution function

In accordance to the Chapman-Enskog procedure (section 5.1), the equilibrium distribution function should satisfy the following constraints:

$$\begin{aligned} \sum_{a=0}^b f_a^{\text{eq}} &= \rho && \text{'Mass conservation'} \\ \sum_{a=0}^b f_a^{\text{eq}} e_{a_i} &= \rho u_i && \text{'Momentum conservation'} \\ \underbrace{\sum_{a=0}^b f_a^{\text{eq}} e_{a_i} e_{a_j}}_{\Pi_{i,j}^{\text{eq}}} &= P_{i,j} + \rho u_i u_j && \text{'Momentum flux tensor'} \\ \underbrace{\sum_{a=0}^b f_a^{\text{eq}} e_{a_i} e_{a_j} e_{a_k}}_{\mathcal{D}_{i,j,k}^{\text{eq}}} &= \mathcal{M}(u_i \delta_{jk} + u_j \delta_{ik} + u_k \delta_{ij}) && \text{'Constitutive physics'} \end{aligned} \quad (\text{B.1})$$

where \mathcal{M} and $P_{i,j}$ are the coefficient related to the fluid viscosity and pressure tensor, respectively.

TABLE 1*Symmetry characteristics of the most commonly used lattices.*

<i>Lattice</i>	<i>Order of symmetry</i>	<i>r</i>	<i>w_a^{b,c}</i>	$\Upsilon^{(2)d,e}$	$\Upsilon^{(4)}$	\mathbf{e}_a/c
D_2Q_7	4^{th}	2	$w_0 = var = \{\frac{1}{2}\}$ $w_{a \neq 0} = \frac{1-w_0}{6}$	$3c^2$	$\frac{3}{4}c^4$	(0,0) $(\cos \frac{2\pi a}{6}, \sin \frac{2\pi a}{6})$
D_2Q_9 Fig.1a	4^{th}	3	$w_0 = var = \{\frac{4}{9}\}$ $w_a^{orth} = 4w_a^{diag}$ $w_a^{diag} = \frac{1-w_0}{20}$	$\frac{3(1-w_0)}{5}c^2$	$\frac{1-w_0}{5}c^4$	(0,0) cyc.($\pm 1, 0$) ($\pm 1, \pm 1$)
D_3Q_{15} Fig.1b	4^{th}	3	$w_0 = var = \{\frac{1}{8}\}$ $w_a^{orth} = 8w_a^{diag}$ $w_a^{diag} = \frac{1-w_0}{56}$	$\frac{3(1-w_0)}{7}c^2$	$\frac{1-w_0}{7}c^4$	(0,0,0) cyc.($\pm 1, 0, 0$) ($\pm 1, \pm 1, \pm 1$)

^a $D_{\mathcal{D}}Q_{b+1}$, where \mathcal{D} is a dimension and b is the total number of moving directions.^b The most commonly used values are given in brackets.^c Note: $\sum_a w_a = 1$.^d $c = \frac{\delta_x}{\delta_t}$, where δ_x and δ_t are the length and time scales, correspondingly.^e Note that the pressure constitutes the diagonal part of the fluid's stress tensor. Thus, the coefficient before the second-order Kroenecker symbol $\delta_{i,j}$ is the lattice pseudo-sound-speed, $\Upsilon^{(2)} \equiv c_s^2$.

The equilibrium distribution function may be approximated by series of Chapman-Enskog expansions in macroscopic variables, to the second order, in the low-Mach-number limit:

$$f_{a \neq 0}^{\text{eq}} = \rho w_a [A + B e_{a_i} u_i + C u^2 + D e_{a_i} e_{a_j} u_i u_j + \dots] \quad (\text{B.2})$$

$$f_0^{\text{eq}} = \rho w_0 [A_0 + C_0 u^2 + \dots]$$

Using the symmetry properties of the lattice given in appendix A, one can show that the constraints eq.(B.1) are satisfied with the following parameters of the expansion [74]:

$$A + C u^2 = \frac{2c_s^2 - u^2}{2\Upsilon^{(2)}} + \beta \quad (\text{B.3})$$

$$B = \frac{1}{\Upsilon^{(2)}} \quad (\text{B.4})$$

$$D u_i u_j = \frac{u_i u_j}{2\Upsilon^{(4)}} + \frac{1}{2\rho\Upsilon^{(4)}} \left[P_{ij}^* - \frac{\text{Tr}(P^*)}{2 + \mathcal{D}} \delta_{ij} - \rho\beta\Upsilon^{(2)} \frac{2}{2 + \mathcal{D}} \delta_{ij} \right] \quad (\text{B.5})$$

$$A_0 + C_0 u^2 = \frac{1}{w_0} \left[1 - (1 - w_0) \frac{2c_s^2 - u^2}{2\Upsilon^{(2)}} - \frac{u^2 \Upsilon^{(2)}}{2\Upsilon^{(4)}} - \right. \quad (\text{B.6})$$

$$\left. - \frac{\Upsilon^{(2)}}{\Upsilon^{(4)}(2 + \mathcal{D})} [\text{Tr}(P^*) - \rho\beta\mathcal{D}\Upsilon^{(2)}] - \rho\beta(1 - w_0) \right] \quad (\text{B.7})$$

where β is a free parameter, \mathcal{D} is a space dimension, and $Tr(P^*)$ is a trace of the nonideal part of the pressure tensor, $P_{i,j}^* = P_{i,j} - \rho c_s^2 \delta_{i,j}$.

Coefficient \mathcal{M} is given by:

$$\mathcal{M} = \rho \frac{\Upsilon^{(4)}}{\Upsilon^{(2)}} \quad (\text{B.8})$$

Setting $\beta = 0$ and $P_{i,j}^* = 0$ ('ideal fluid'), we can write f_a^{eq} in the following compact form:

$$\begin{aligned} f_0^{\text{eq}} &= \rho \left[1 - \frac{1-w_0}{\Upsilon^{(2)}} c_s^2 - \frac{u^2}{2} \left(\frac{\Upsilon^{(2)}}{\Upsilon^{(4)}} - \frac{1-w_0}{\Upsilon^{(2)}} \right) \right] \\ f_{a \neq 0}^{\text{eq},0} &= \rho w_a \left[\frac{c_s^2}{\Upsilon^{(2)}} - \frac{u^2}{2\Upsilon^{(2)}} + \frac{e_{a_i} u_i}{\Upsilon^{(2)}} + \frac{e_{a_i} e_{a_j} u_i u_j}{2\Upsilon^{(4)}} \right] \end{aligned} \quad (\text{B.9})$$

which are exactly the same equations as given in the LBE literature, [19] and [77]. Using the pressure tensor given by eq.(51) and the following equation for β :

$$\beta = \frac{P_0^* - \kappa \rho \partial_{kk} \rho + \left(\frac{1}{\mathcal{D}} - \frac{1}{2} \right) \kappa (\partial_k \rho)^2}{\Upsilon^{(2)} \rho} \quad (\text{B.10})$$

where $P_0^* = P_0 - \rho c_s^2$ is a 'nonideal part' of the equation of state, one can obtain the 'free-energy-based' LBE model for 'non-ideal fluid' of Swift et al. [97].

In the 'ideal fluid' model, the lattice 'pseudo-sound-speed' is a function of the lattice size and time step, δ_x and δ_t , and the weight of the non-moving populations, w_0 , see Table 1. In the LBE literature, the value of w_0 is chosen in order to remove non-Navier-Stokes terms from the hydrodynamic equivalent of the LBE models. For the D_2Q_9 model, $w_0 = \frac{4}{9}$, [77]. In this case, the non-dimensional 'pseudo-sound-speed' is $\left(\frac{c_s}{c} \right)^2 = \frac{1}{3}$.

APPENDIX C

Multiphase flow modeling

In this section, we provide a classification of the methods of computational fluid dynamics (CFD) for multiphase, fluid-fluid flow. We will discuss only the 'direct numerical simulation' (DNS) methods (i.e., those which resolve interface), putting aside 'effective field' methods, which employ statistically-, time- or spatially-averaged equations for multiphase systems ([24] [51]). The chief criterion used to classify a CFD method for DNS in multiphase flow is the physical concept of interfaces.

1. **"Free-Boundary Approach", FBA.** In this approach the interface between two immiscible fluids is a free boundary which evolves in time. Equations of fluid motion hold in each fluid. These equations are supplemented by boundary conditions at the free surface, involving interfacial properties⁴⁴. The formulation results in a free-boundary problem

⁴⁴This approach originates from earliest works of Young, Laplace and Gauss, in 1800's. They considered the interface between two fluids as a surface of zero thickness endowed with physical properties such as surface tension.

(Lamb, 1932 [61], Batchelor, 1967 [6], etc.). Physical quantities, e.g. density and viscosity, are discontinuous across the interface. Physical processes such as e.g. capillarity occurring at the interface, are represented by the boundary (“jump”) conditions imposed there. Computational methods based on the “free-boundary” concept are the *boundary element/boundary integral method*, (BE/BIM) ([85] [105]).

2. **“Physical-Diffuse-Interface Approach”, PDIA** [4]. This approach is based on the Poisson’s (1831) [81] Maxwell’s (1876) [68] and Gibbs’s (1876) [32] concept of the interface as a rapid and smooth transition of physical properties between the bulk fluid values. The approach was further developed by Rayleigh (1892) [82] and van der Waals (1893) [100] with their “gradient theories for the interface” based on the thermodynamic principles, and Korteweg (1901) [56], who proposed a constitutive law for the capillary stress tensor in terms of the density and its spatial gradients. Corresponding CFD methods are the “second-gradient theory”, “phase-field” and “Model H” [47]. They all are based on the “continuum mechanics methodology”, in which transport equations for macroscopic variables are constructed, introducing the phenomenological physical models for interfacial dynamics through the effective forcing terms in the momentum equations (“capillary stress tensors”, “free-energy” concept, Cahn-Hilliard’s approach, etc.) and additional evolution equations for “order” parameters. The “PDIA” CFD methods were used in a number of applications, including studies of critical point scaling laws [47], capillary waves [29], moving contact lines [87], droplets and nucleation [22], droplet breakup [52] and spinoidal decomposition [37] (see for review [4]).

3. **“Numerical-Diffuse-Interface Approach”, NDIA**. The methods of this group involve a numerical scheme to “capture” or “track” the interface. The interface region is numerically smeared-out over few computational nodes to allow a smooth transition of fluid properties (i.e., density and viscosity). In this “numerical diffuse interface” region, the capillary effects are represented by “body forces” in the momentum equation, which mimic the Korteweg’s capillary stress tensor. Advanced CFD developments in this class were made with the “volume-of-fluid” method, VOF [46]; the level set equation method, LSA, [88]; and the “front-tracking” technique by Tryggvason [99].

APPENDIX D

Derivation of the viscous stress tensor for the LBGK models

In this section, we show the derivation of the viscous tensor for a LBGK model and detailed formula for two other LBGK models. The non-Navier-Stokes terms are grouped into an artifact tensor to enable a further assessment of the hydrodynamic equivalent of the LBE models.

Isothermal ideal gas.

$$\begin{aligned}
\partial_j \mathcal{T}_{i,j}^{\text{LBGK}} &= -\partial_j \varepsilon \mathcal{P}_{i,j}^{(1)} = -\partial_j \varepsilon \underbrace{\sum_a (e_{a_i} - u_i)(e_{a_j} - u_j) f_a^{(1)}}_{\mathcal{P}_{i,j}^{(1)} = \sum_a e_{a_i} e_{a_j} f_a^{(1)}} = \\
&= \left[\dots f_a^{(1)} = \text{eq.(79)} = -\tau \left(\partial_{t_0} f_a^{(0)} + e_{a_k} \partial_k f_a^{(0)} - \frac{a_k}{c_s^2} (e_{a_k} - u_k) f_a^{(0)} \right) \dots \right] = \quad (\text{D.1}) \\
&= \tau \varepsilon \partial_j \left(\underbrace{\partial_k \mathcal{D}_{i,j,k}^{(0)}}_{(\text{A})} + \underbrace{\partial_{t_0} \Pi_{i,j}^{(0)}}_{(\text{B})} - \underbrace{\frac{a_k}{c_s^2} \left(\mathcal{D}_{i,j,k}^{(0)} - u_k \Pi_{i,j}^{(0)} \right)}_{(\text{C}) \rightarrow \text{A}_{i,j} = \text{Artifact}} \right)
\end{aligned}$$

$\mathcal{D}_{i,j,k}^{(0)}$ and $\Pi_{i,j}^{(0)}$ are given by eq.(B.1).

$$\begin{aligned}
(\text{A}) : \quad \partial_j \partial_k \left[\underbrace{\tau \varepsilon \rho \frac{\Upsilon^{(4)}}{\Upsilon^{(2)}}}_{=\hat{\mathcal{M}}, \text{ eq.(B.8)}} (u_i \delta_{j,k} + u_j \delta_{i,k} + u_k \delta_{i,j}) \right] = \quad (\text{D.2}) \\
= \underbrace{\partial_j \left[\hat{\mathcal{M}} (\partial_j u_i + \partial_i u_j) + \hat{\mathcal{M}} \cdot \partial_k u_k \cdot \delta_{i,j} \right]}_{\rightarrow \mathcal{T}_{i,j} = \text{N.S. viscous stress tensor}} + \underbrace{\partial_j \left[u_i \partial_j \hat{\mathcal{M}} + u_j \partial_i \hat{\mathcal{M}} + u_k \cdot \partial_k \hat{\mathcal{M}} \cdot \delta_{i,j} \right]}_{\rightarrow \text{A}_{i,j} = \text{Artifact}}
\end{aligned}$$

Shear viscosity can be identified as

$$\eta = \hat{\mathcal{M}} = \tau \varepsilon \rho \frac{\Upsilon^{(4)}}{\Upsilon^{(2)}} \quad (\text{D.3})$$

and

$$\tau \varepsilon = \nu \frac{\Upsilon^{(2)}}{\Upsilon^{(4)}}, \quad \nu = \frac{\eta}{\rho} = \text{const} \quad (\text{D.4})$$

$$\begin{aligned}
(\text{B}) : \quad \nu \frac{\Upsilon^{(2)}}{\Upsilon^{(4)}} \partial_j \left[\underbrace{c_s^2 \partial_{t_0} \rho \delta_{i,j}}_{-c_s^2 \partial_k \rho u_k \delta_{i,j}, \text{ eq.(73)}} + \partial_{t_0} \rho u_i u_j \right] = \\
= \nu \frac{\Upsilon^{(2)}}{\Upsilon^{(4)}} \partial_j \left[\underbrace{-\rho c_s^2 \partial_k u_k \delta_{i,j}}_{\rightarrow \mathcal{T}_{i,j}} - \underbrace{c_s^2 u_k \partial_k \rho \delta_{i,j}}_{\rightarrow \text{A}_{i,j}} + \underbrace{u_i \partial_{t_0} \rho u_j + u_j \partial_{t_0} \rho u_i}_{\substack{\text{eq.(74)} \\ \rightarrow \text{A}_{i,j}}} \right] \quad (\text{D.5})
\end{aligned}$$

Combining all terms, the viscous stress tensor is given by

$$\partial_j \mathcal{T}_{i,j}^{\text{LBGK}} = \partial_j \left[\eta (\partial_j u_i + \partial_i u_j) + \left(\eta - \eta c_s^2 \frac{\Upsilon^{(2)}}{\Upsilon^{(4)}} \right) \partial_k u_k \cdot \delta_{i,j} \right] \quad (\text{D.6})$$

yielding the second viscosity given by eq.(84). The remaining terms are agglomerated into the ‘artifact’ tensor:

$$\begin{aligned} A_{i,j} = & \nu \partial_j [u_i \partial_j \rho + u_j \partial_i \rho + u_k \partial_k \rho \delta_{i,j}] + \\ & + \nu \frac{\Upsilon^{(2)}}{\Upsilon^{(4)}} \partial_j [-c_s^2 u_k \partial_k \rho \delta_{i,j} + u_i (-\partial_k \rho u_k u_j - c_s^2 \partial_j \rho + \rho a_j) + \\ & + u_j (-\partial_k \rho u_k u_i - c_s^2 \partial_i \rho + \rho a_i) \\ & - \frac{a_k}{c_s^2} \left(\rho \frac{\Upsilon^{(4)}}{\Upsilon^{(2)}} (u_i \delta_{j,k} + u_j \delta_{i,k} + u_k \delta_{i,j}) - u_k (\rho c_s^2 \delta_{i,j} + \rho u_i u_j) \right)] \end{aligned} \quad (D.7)$$

which, by setting $\frac{\Upsilon^{(4)}}{\Upsilon^{(2)}} = c_s^2$, can be re-arranged to produce the non-linear deviation term given by eq.(88).

Free-energy-based model for non-ideal fluid. Repeating the calculations presented above⁴⁵, the following viscosities and “artifact” terms are obtained:

$$\eta = \tau \varepsilon \rho \frac{\Upsilon^{(4)}}{\Upsilon^{(2)}}; \quad \xi = \eta \left(\frac{5}{3} + \frac{\Upsilon^{(2)}}{\Upsilon^{(4)}} \left(2a\rho - \frac{c_s^2}{1-b\rho} - \frac{\rho c_s^2 b}{(1-b\rho)^2} + \kappa \partial_l^2 \rho \right) \right) \quad (D.8)$$

$$\begin{aligned} A_{i,j} = & \nu \frac{\Upsilon^{(2)}}{\Upsilon^{(4)}} \left\{ \partial_j \left[\left(2a\rho - \frac{c_s^2}{1-b\rho} - \frac{\rho c_s^2 b}{(1-b\rho)^2} \right) u_k + \kappa (u_k \partial_l^2 \rho + \partial_{kl} \rho u_l) \right] \partial_k \rho \delta_{i,j} \right. \\ & - \partial_i \rho \left[\kappa \partial_{jk} \rho u_k + u_j \left(\frac{c_s^2}{1-b\rho} + \frac{\rho c_s^2 b}{(1-b\rho)^2} \right) - 2a\rho u_j \right] - \\ & - \partial_j \rho \left[\kappa \partial_{ik} \rho u_k + u_i \left(\frac{c_s^2}{1-b\rho} + \frac{\rho c_s^2 b}{(1-b\rho)^2} \right) - 2a\rho u_i \right] - \\ & \left. - [u_i \partial_k u_k u_j + u_j \partial_k u_k u_i] \cdot \partial_j \rho \right\} - \eta \frac{\Upsilon^{(2)}}{\Upsilon^{(4)}} \partial_j [u_i \partial_k u_k u_j + u_j \partial_k u_k u_i] \end{aligned} \quad (D.9)$$

“HSD” model for non-ideal fluid. The following “artifact” term is obtained for the “HSD” model:

$$\begin{aligned} A_{i,j} = & -\nu \frac{\Upsilon^{(2)}}{\Upsilon^{(4)}} \left\{ \partial_j \left[\left(c_s^2 - \frac{\Upsilon^{(4)}}{\Upsilon^{(2)}} \right) (u_k \partial_k \rho \delta_{i,j} + u_i \partial_j \rho + u_j \partial_i \rho) - \right. \right. \\ & - \left(2a\rho + c_s^2 - \frac{c_s^2}{1-b\rho} - \frac{\rho c_s^2 b}{(1-b\rho)^2} \right) \left(\frac{u_i u_j u_k}{c_s^2} \partial_k \rho + \left(1 - \frac{\Upsilon^{(4)}}{\Upsilon^{(2)} c_s^2} \right) \cdot \right. \\ & \cdot (u_i \partial_j \rho + u_j \partial_i \rho + u_k \partial_k \rho \delta_{i,j}) - \rho \kappa [u_i \partial_j^3 \rho + u_j \partial_i^3 \rho + \partial_k \partial_i^2 \rho \cdot \\ & \cdot (u_k (1 - \frac{\Upsilon^{(4)}}{\Upsilon^{(2)} c_s^2}) \delta_{i,j} + \frac{u_i u_j u_k}{c_s^2}) - \frac{\Upsilon^{(4)}}{\Upsilon^{(2)} c_s^2} (u_i \partial_j \partial_k^2 \rho + u_j \partial_i \partial_k^2 \rho)] \\ & \left. \left. + 2u_i u_j u_k \partial_k \rho \right] - \right. \\ & \left. - \partial_j \rho \left[\left(1 - \frac{\Upsilon^{(4)}}{\Upsilon^{(2)} c_s^2} \right) (u_i g_j + u_j g_i + u_k g_k \delta_{i,j}) + \frac{u_i u_j u_k}{c_s^2} g_k - u_i \partial_k u_j u_k - u_j \partial_k u_i u_k \right] \right\} + \\ & + \eta \partial_j \left[\left(\frac{\Upsilon^{(2)}}{\Upsilon^{(4)}} - \frac{1}{c_s^2} \right) (u_i g_j + u_j g_i + u_k g_k \delta_{i,j}) \right. \\ & \left. + \frac{\Upsilon^{(2)}}{\Upsilon^{(4)}} \left(\frac{u_i u_j u_k g_k}{c_s^2} - u_i \partial_k u_j u_k - u_j \partial_k u_i u_k \right) \right] \end{aligned} \quad (D.10)$$

⁴⁵In this derivation though, for simplicity, we neglected the derivatives of the third and higher order. Strictly speaking, this is not well grounded, because the momentum conservation equation (96) contains terms of the third-order derivative of density.

APPENDIX E

Evaluation of the deviations from the Navier-Stokes equations

IDEAL GAS MODELS

To estimate the order of the non-linear deviation term, we cast the LBGK hydrodynamic equation (89) into the following dimensional form:

$$\begin{aligned}
 & \underbrace{\frac{\partial_t \rho u_i}{\sim \mathbb{O}(1 + \delta \rho_i)}} + \underbrace{\frac{\partial_j \rho u_i u_j}{\sim \mathbb{O}(1 + \delta \rho_L)}} = \partial_i P + \underbrace{\frac{\rho a_i}{\sim \mathbb{O}\left(\frac{1}{Fr}\right)}} + \\
 & + \underbrace{\partial_j [\rho \nu (\partial_j u_i + \partial_i u_j)]}_{\sim \mathbb{O}\left(\frac{1 + \delta \rho_L}{Re}\right)} + \underbrace{A_{i,j}^{(n.l.d.)}}_{\sim \mathbb{O}\left(\frac{(1 + \delta \rho_L)}{Re \, c_s^2}\right)} \text{ and } \underbrace{\sim \mathbb{O}\left(\frac{(1 + \delta \rho_L)}{c_s^4 Re Fr}\right)}
 \end{aligned} \tag{E.1}$$

where the Froude number is defined as $Fr \equiv \frac{U_0^2}{aL}$; and a is an acceleration due to the external body force. The non-dimensional density variations are defined by eq.(93) and (94). It can be seen that the non-linear deviation term is negligibly small comparing to the Navier-Stokes equation terms under conditions⁴⁶ $\hat{c}_s \gg 1$ (or $\Upsilon^{(2)} \gg 1$, see Table 1).

In difference to our derivation, the LBGK hydrodynamic equations available in the literature contain also *linear deviations*. For example, re-arranging the LBGK hydrodynamic equations given in [16] and [77] in a similar way as eq.(E.1), one can obtain the following “linear deviation term”:

$$A_{i,j}^{(l.d.)} = \underbrace{\nu [\partial_j \rho \cdot (2\partial_j u_i + \partial_i u_j) + \partial_i \rho \cdot \partial_j u_j + u_i \partial_j^2 \rho + u_j \partial_i \partial_j \rho]}_{\sim \mathbb{O}\left(\frac{\delta \rho_L}{Re}\right)} \tag{E.2}$$

which is negligible in comparison to the Navier-Stokes terms in the limit $\delta \rho_L \ll 1$.

The following linear and non-linear deviations can be obtained by re-arranging the LBGK hydrodynamic equations of ref. [78]:

$$\begin{aligned}
 A_{i,j}^{(l.d.)} &= \underbrace{\nu \partial_j \rho \cdot (\partial_j u_i + \partial_i u_j)}_{\sim \mathbb{O}\left(\frac{\delta \rho_L}{Re}\right)}; & A_{i,j}^{(n.l.d.)} &= \underbrace{-\nu \partial_j \partial_k \frac{\rho u_i u_j u_k}{c_s^2}}_{\sim \mathbb{O}\left(\frac{\delta \rho_L}{c_s^2 Re}\right)}
 \end{aligned} \tag{E.3}$$

Both the linear and non-linear terms are negligible under conditions $\delta \rho_L \ll 1$ and $\hat{c}_s \gg 1$.

⁴⁶Recently, Qian and Zhou [79] explored a way to eliminate the non-linear term by extending the “lattice stencil” from 9 to 17 discrete velocities in 2D case.

Compressibility effects. It can be seen that the LBE model is not actually incompressible in a “classical” fluid dynamics sense, which requires the velocity field be solenoidal $\nabla \cdot \mathbf{u} = 0$ and $\rho = \text{const.}$ There are always density variations and velocity divergence sources present, due to the linearized “pseudo equation of state” $P = c_s^2 \rho$ (see eqs.(E.5) and (E.6)). The undesirable compressibility effects are minor as long as density variations are small^{47,48}, $\sim \mathbb{O}(\delta \rho_t)$, $\sim \mathbb{O}(\delta \rho_l)$, $\sim \mathbb{O}\left(\frac{\delta \rho_l}{\text{Re}}\right)$, and thermodynamic effects are not considered.

$$\begin{array}{c} \text{Velocity} \\ \text{divergence sources} \end{array} \quad \underbrace{\partial_j u_j}_{\sim \mathbb{O}(1)} = \underbrace{\underbrace{-\partial_t \ln \rho}_{\sim \mathbb{O}(\delta \rho_t)} \underbrace{-u_j \partial_j \ln \rho}_{\sim \mathbb{O}(\delta \rho_l)}}_{\text{Compressibility effects (Mass)}} \sim \mathbb{O}(\max[\delta \rho_t, \delta \rho_l]) \quad (\text{E.5})$$

Incompressible Navier-Stokes Part	$\underbrace{\partial_t u_i}_{\sim \mathbb{O}(1)} + \underbrace{u_j \partial_j u_i}_{\sim \mathbb{O}(1)} = -\frac{\partial_i P}{\rho} \underbrace{+ a_i}_{\sim \mathbb{O}\left(\frac{1}{\text{Fr}}\right)} + \underbrace{\partial_j [\nu (\partial_j u_i + \partial_i u_j)]}_{\sim \mathbb{O}\left(\frac{1}{\text{Re}}\right)}$
Deviation from Incompressible Navier-Stokes	<div style="text-align: center; margin-bottom: 10px;"> Compressibility effects (Momentum) </div> $\underbrace{\underbrace{-u_i \partial_t \ln \rho}_{\sim \mathbb{O}(\delta \rho_t)} \underbrace{-\frac{u_i \partial_j \rho u_j}{\rho}}_{\sim \mathbb{O}(\max[\delta \rho_t, \delta \rho_l])}}_{\text{Compressibility effects (Momentum)}} + \underbrace{\nu (\partial_j u_i + \partial_i u_j) \cdot \partial_j \ln \rho}_{\sim \mathbb{O}\left(\frac{\delta \rho_l}{\text{Re}}\right)} \quad (\text{E.6})$ <hr/> <div style="text-align: center;"> Non-linear deviation: $\sim \mathbb{O}\left(\frac{(1+\delta \rho_t)}{c_s^2 \text{Re}}\right)$ and $\sim \mathbb{O}\left(\frac{(1+\delta \rho_l)}{c_s^2 \text{Re Fr}}\right)$ $+ A_{i,j}^{(\text{n.l.d.})} / \rho$ </div>

⁴⁷ Several LBGK models were developed in an attempt to reduce these compressibility effects [18] [41]. In particular, He and Luo [41] utilized the Chorin’s “pseudo-compressibility” method [20], in which instead of eq.(63) the following macroscopic ‘pressure’ equation is introduced:

$$\frac{1}{c_s^2} \partial_t P + \partial_j u_j = 0 \quad (\text{E.4})$$

Instead of the mass and momentum, the P and $P\mathbf{u}$ are conserved. Eqs.(E.4) and (83) become a ‘target’ macroscopic model for the “heuristic” building of the equilibrium distribution function. In the case of the steady flow, this model completely recovers the ‘divergence-free’ velocity field. In the case of the transient flow, the requirement $\delta \rho_t \ll 1$ is still necessary to keep the divergence sources be suppressed.

⁴⁸ Another “incompressible” LBE model is due to Chen and Ohashi [18], in which the incompressibility condition $\nabla \cdot \mathbf{u}$ is regained by applying the velocity correction - an idea borrowed from the ‘projection’ methods [83].

FREE-ENERGY BASED MODELS

The “linear deviation tensor” of the free-energy-based model of the Swift et al. can be written in the following form:

$$\begin{aligned}
 \mathbf{A}_{i,j}^{(l.d.)} = & \frac{\nu}{c_s^2} \left\{ \partial_j \left[\left(\underbrace{\left(2a\rho - \frac{c_s^2}{1-b\rho} - \frac{\rho c_s^2 b}{(1-b\rho)^2} \right) u_k}_{\sim \mathbb{O}\left(\frac{\delta\rho_l}{\text{Re}}\right)} + \underbrace{\kappa (u_k \partial_l^2 \rho + \partial_{kl} \rho u_l)}_{\sim \mathbb{O}\left(\frac{\delta\rho_l}{c_s^2 \text{ReWe}}\right)} \right] \partial_k \rho \delta_{i,j} - \right. \\
 & - \partial_i \rho \left[\underbrace{\kappa \partial_{jk} \rho u_k}_{\sim \mathbb{O}\left(\frac{\delta\rho_l}{c_s^2 \text{ReWe}}\right)} + \underbrace{u_j \left(\frac{c_s^2}{1-b\rho} + \frac{\rho c_s^2 b}{(1-b\rho)^2} \right) - 2a\rho u_j}_{\sim \mathbb{O}\left(\frac{\delta\rho_l}{\text{Re}}\right)} \right] - \\
 & \left. - \partial_j \rho \left[\underbrace{\kappa \partial_{ik} \rho u_k}_{\sim \mathbb{O}\left(\frac{\delta\rho_l}{c_s^2 \text{ReWe}}\right)} + \underbrace{u_i \left(\frac{c_s^2}{1-b\rho} + \frac{\rho c_s^2 b}{(1-b\rho)^2} \right) - 2a\rho u_i}_{\sim \mathbb{O}\left(\frac{\delta\rho_l}{\text{Re}}\right)} \right] \right\} \quad (\text{E.7})
 \end{aligned}$$

and the “non-linear deviation tensor” is:

$$\begin{aligned}
 \mathbf{A}_{i,j}^{(n.l.d.)} = & -\frac{\eta}{c_s^2} \partial_j [u_i \partial_k u_k u_j + u_j \partial_k u_k u_i] - \\
 & - \frac{\nu}{c_s^2} \underbrace{\{ \partial_j [\partial_k \rho \cdot 2u_i u_j u_k] + [u_i \partial_k u_k u_j + u_j \partial_k u_k u_i] \cdot \partial_j \rho \}}_{\sim \mathbb{O}\left(\frac{(1+\delta\rho_l)}{c_s^2 \text{Re}}\right)} \quad (\text{E.8})
 \end{aligned}$$

The linear deviation term includes the unphysical capillary terms of order $\sim \mathbb{O}\left(\frac{\delta\rho_l}{c_s^2 \text{ReWe}}\right)$. Comparison of these terms with the capillary stress tensor and the Navier-Stokes viscous stress tensor gives

$$\frac{\mathbf{A}_{i,k}^{(l.d.)}}{\mathbf{K}_{i,k}} \sim \mathbb{O}\left(\frac{1}{\hat{c}_s^2 (1 + \delta\rho_l) \text{Re}}\right)$$

and

$$\frac{A^{(l.d.)}_{i,k}}{\partial_j \mathcal{T}_{i,j}} \sim \mathbb{O} \left(\frac{\delta \rho_l}{1 + \delta \rho_l} \frac{1}{\hat{c}_s^2 We} \right)$$

which indicates that in order to have the unphysical surface tension suppressed, one has to keep large \hat{c}_s .

Furthermore, the “linear deviation term” includes terms of unphysical viscous stresses of the order $\sim \mathbb{O} \left(\frac{\delta \rho_l}{Re} \right)$. Comparison of these “artifacts” with the Navier-Stokes viscous stress tensor:

$$\frac{A^{(l.d.)}_{i,k}}{\partial_j \mathcal{T}_{i,j}} \sim \mathbb{O} \left(\frac{\delta \rho_l}{1 + \delta \rho_l} \right)$$

indicates that these unphysical terms cannot be neglected for large density differences $\rho_l - \rho_v$, even for conditions of large ‘pseudo-sound-speed’, $\hat{c}_s \gg 1$. This is one of the reasons why this LBGK scheme suffers from few unphysical effects, such as Galilean invariance problem, [97] and section 4.7.2.

Non-linear deviation. Unphysical viscous stresses due to the non-linear deviation can be suppressed by keeping large ‘pseudo-sound-speed’, $\hat{c}_s \gg 1$,

$$\frac{A^{(n.l.d.)}_{i,k}}{K_{i,k}} \sim \mathbb{O} \left(\frac{We}{\hat{c}_s^2 \delta \rho_l} \right) \quad \text{and} \quad \frac{A^{(n.l.d.)}_{i,k}}{\partial_j \mathcal{T}_{i,j}} \sim \mathbb{O} \left(\frac{1}{\hat{c}_s^2} \right)$$

HE-SHAN-DOOLEN MODEL

The “linear deviation” tensor is:

$$A^{(l.d.)}_{i,j} = - \frac{\nu}{\hat{c}_s^2} \underbrace{\left\{ \partial_j \left[-\rho \kappa \left[u_i \partial_j^3 \rho + u_j \partial_i^3 \rho - (u_i \partial_j \partial_k^2 \rho + u_j \partial_i \partial_k^2 \rho) \right] \right] \right\}}_{\sim \mathbb{O} \left(\frac{\delta \rho_l (1 + \delta \rho_l)}{\hat{c}_s^2 Re We} \right)} \quad (E.9)$$

Comparing this unphysical term with capillary and viscous stress tensors:

$$\begin{aligned} \frac{A^{(l.d.)}_{i,j}}{K_{i,j}} &\sim \mathbb{O} \left(\frac{(1 + \delta \rho_l)}{\hat{c}_s^2 Re} \right) \\ \frac{A^{(l.d.)}_{i,j}}{\partial_j \mathcal{T}_{i,j}} &\sim \mathbb{O} \left(\frac{\delta \rho_l}{\hat{c}_s^2 We} \right) \end{aligned} \quad (E.10)$$

indicates that keeping large $\hat{c}_s \gg 1$, this “artifact” can be considered as negligibly small, even for large density ratios $\frac{\rho_l}{\rho_v} \gg 1$, which is significant improvement in comparison to the “free-energy-based” approach.

The “non-linear deviation” tensor is given by the following equation:

$$\begin{aligned}
\mathbf{A}_{i,j}^{(\text{n.l.d.})} = & -\frac{\nu}{c_s^2} \left\{ \partial_j \left[\underbrace{- \left(2a\rho + c_s^2 - \frac{c_s^2}{1-b\rho} - \frac{\rho c_s^2 b}{(1-b\rho)^2} \right) \frac{u_i u_j u_k}{c_s^2} \partial_k \rho}_{\sim \mathbb{O} \left(\frac{\delta \rho_L}{\hat{c}_s^2 \text{Re}} \right)} - \right. \right. \\
& \left. \underbrace{- \rho \kappa \left[(\partial_k \partial_l^2 \rho) \frac{u_i u_j u_k}{c_s^2} \right]}_{\sim \mathbb{O} \left(\frac{\delta \rho_L (1+\delta \rho_L)}{\hat{c}_s^4 \text{ReWe}} \right)} + \underbrace{2u_i u_j u_k \partial_k \rho}_{\sim \mathbb{O} \left(\frac{\delta \rho_L}{\hat{c}_s^2 \text{Re}} \right)} \right. \\
& \left. - \partial_j \rho \left[\underbrace{\frac{u_i u_j u_k}{c_s^2} g_k}_{\sim \mathbb{O} \left(\frac{\delta \rho_L}{\hat{c}_s^4 \text{ReFr}} \right)} - \underbrace{u_i \partial_k u_j u_k - u_j \partial_k u_i u_k}_{\sim \mathbb{O} \left(\frac{\delta \rho_L}{\hat{c}_s^2 \text{Re}} \right)} \right] \right\} + \\
& + \frac{\eta}{c_s^2} \partial_j \left[\underbrace{\frac{u_i u_j u_k g_k}{c_s^2}}_{\sim \mathbb{O} \left(\frac{1}{\hat{c}_s^4 \text{ReFr}} \right)} - \underbrace{u_i \partial_k u_j u_k - u_j \partial_k u_i u_k}_{\sim \mathbb{O} \left(\frac{1}{\hat{c}_s^2 \text{Re}} \right)} \right]
\end{aligned} \tag{E.11}$$

and includes terms of order $\sim \mathbb{O} \left(\frac{1+\delta \rho_L + \delta \rho_L^2}{\hat{c}_s^4 \text{ReWe}} \right)$ and $\sim \mathbb{O} \left(\frac{1+\delta \rho_L}{\hat{c}_s^2 \text{Re}} \right)$, which allows to make this unphysical term be suppressed by keeping the limit $\hat{c}_s \gg 1$.